Image charge effects in ion surface scattering

1996 J. Phys.: Condens. Matter 8 10149

(http://iopscience.iop.org/0953-8984/8/49/009)

J. Phys.: Condens. Matter **8** (1996) 10149–10183. Printed in the UK

REVIEW ARTICLE

Image charge effects in ion surface scattering

H Winter

Institut für Physik, Humboldt-Universität zu Berlin, Invalidenstraße 110, D-10115 Berlin, Germany

Received 3 September 1996

Abstract. Image charge effects on the trajectories of fast ions during the grazing scattering from a solid surface are discussed. It is shown that these effects can be made use of in detailed studies on charge exchange phenomena in front of a surface. In some detail we shall outline recent progress in studies on 'skipping motion' and on the neutralization of multicharged ions.

1. Introduction

When a charged particle is brought close to a solid surface, the dielectric response of the medium leads to a polarization potential that acts back on the external charge. This feature is well known from classical electrostatics, where it is described by the concept of 'image charge' (Jackson 1975). It turns out that this concept can be applied to a wide extent also on microscopic scales as the static limit of the 'dynamical image potential'. Image charge effects play an important role in the understanding of atom–surface interactions, e.g. chemisorption, electronic work function or charge exchange phenomena.

Already in early papers on image potentials for charged microscopic particles in front of a conducting surface, the influence of the image force on the trajectory of particles during the scattering from the surface has been discussed. Muscat and Newns (1979) have calculated the image charge attraction for kiloelectronvolt electrons and the resulting effects on surface plasmon excitation probabilities. For neutral atoms the image charge interaction is reduced to small van der Waals forces studied by Raskin and Kusch (1968) via the deflection of a thermal atomic beam by a curved surface. However, in both cases, no convincing evidence for the effects of image forces could be deduced from the analysis of experimental data. Echenique and Howie (1984) discussed image force effects in electron microscopy and found negligible deflection phenomena for practical applications. The influence of the image charge interaction on ion desorption has been investigated theoretically by Miskovic *et al* (1984).

A peculiar mechanism concerning the image charge interaction of fast ions in front of metal surfaces has been proposed by Ohtsuki *et al* (1979). On the basis of calculations of the dynamical image potential and of computer simulations, these workers predicted for a fraction of the projectiles the hopping type of trajectories in front of the surface plane, the so-called 'skipping motion'. We shall discuss some recent experiments on this subject which give evidence for 'skipping motion' in front of metal and insulator surfaces.

Whereas 'skipping motion' is already a rather sophisticated effect of image (charge) forces on trajectories of fast ions, in recent years considerable progress has been achieved in detailed studies on trajectory effects observed for fast atomic projectiles scattered from

0953-8984/96/4910149+35$19.50

surfaces (Winter 1991, 1992a, Winter and Leuker 1992). In scattering experiments with multiply and highly charged ions those effects have been clearly demonstrated and made use of in investigations on charge exchange phenomena of atoms in front of a surface (Winter 1992b, Winter *et al* 1993). Since the image charge interaction shows a pronounced dependence on the size of the external charge, studies of image force effects on trajectories provide important information on charge transfer. Atomic species (atoms or ions) can bind electrons in states with defined electronic energies. These electrons can be captured or lost by the projectile in the scattering event, resulting in an effective charge of the projectile. In this way, one obtains from image charge effects direct information on distances where charge exchange processes take place. The scattering experiments described below have thus provided additional important information on the atom–surface interaction.

In this brief review on new types of scattering experiment, we first discuss basic features of dielectric response phenomena and of the method, followed by some specific examples of studies on charge transfer of atoms and ions in front of surfaces. We shall then report observations of 'skipping motion' phenomena and describe image charge effects in studies on the neutralization of slow multiply and highly charged ions in front of solid surfaces.

2. Response of a dielectric medium to the presence of an external charge

To a good approximation the effect of an external point charge q in front of a dielectric material can be described without dispersion, i.e. the appropriate dielectric response function is assumed to depend on frequency ω only, represented by a dielectric function $\varepsilon(\boldsymbol{r},\omega) = \varepsilon(\omega)\theta(-z) + \theta(z)$; z is a coordinate normal to the surface plane and $\theta(z)$ a step function. Then the induced potential for a particle moving with velocity $\boldsymbol{v} = (\boldsymbol{v}_p, v_z)$ parallel to the surface at a distance R can be written as (see, e.g., Garcia de Abajo and Echenique (1992) and references therein)

$$V_{in}(\boldsymbol{r},t) = \frac{q}{2\pi}\int \frac{\mathrm{d}\boldsymbol{Q}}{Q}\,\mathrm{e}^{[\mathrm{i}\boldsymbol{Q}\cdot(\boldsymbol{r}-\boldsymbol{v}_p t)-Q(R+z)]}\frac{1-\varepsilon(\omega)}{1+\varepsilon(\omega)} \tag{1}$$

with $\omega = \boldsymbol{Q}\cdot\boldsymbol{v}_p$, where $\boldsymbol{Q}$ denotes the component of momentum $\boldsymbol{k}$ parallel to the surface: $\boldsymbol{k} = (\boldsymbol{Q}, k_z)$. The frequency-dependent dielectric function $\varepsilon(\omega)$ in equation (1) can be deduced from optical constants. For simple metals the classical approximation $\varepsilon(\omega) = 1 - \omega_p^2/\omega(\omega + \mathrm{i}\gamma)$ has been shown to hold astonishingly well (Arista 1994), where $\omega_p = (4\pi n_e)^{1/2}$ is the plasma frequency of the free-electron gas with density n_e and damping constant γ.

It is straightforward to show from equation (1) that the interaction energy to bring a particle with charge q from infinity to a distance $z = R$ converges for sufficiently low v_p and large R to the static classical limit $E_{im} = -q^2/4R$, i.e. $V_{im} = -q/4R$ for the 'image (charge) potential' at a position $\boldsymbol{r} = (\boldsymbol{v}_p t, R)$. In figure 1 we compare the asymptotic limit of V_{im} with potentials derived from equation (1) for a particle with unit charge $q = e = 1$ au moving with velocities $v_p = 1$, 5 and 10 au, respectively, in front of an aluminium surface ($\omega_p = 0.52$ au). From the comparison we conclude for $v_p = 1$ au (e.g. protons with a kinetic energy $E_0 = 25$ keV) that the $1/4R$ approximation is a good description down to distances $z \approx 2$ au; for faster projectiles this approach is poorer and holds only for larger distances.

Note, that the distance R is referred to the 'image plane', located about $z_{im} = 4$ au in front of the topmost layer of surface atoms (Eguiluz and Hanke 1989), and that the potential given by equation (1) remains finite at $R = 0$ in contrast with the classical description. Since for the studies discussed below the relevant distances are larger than some atomic units at

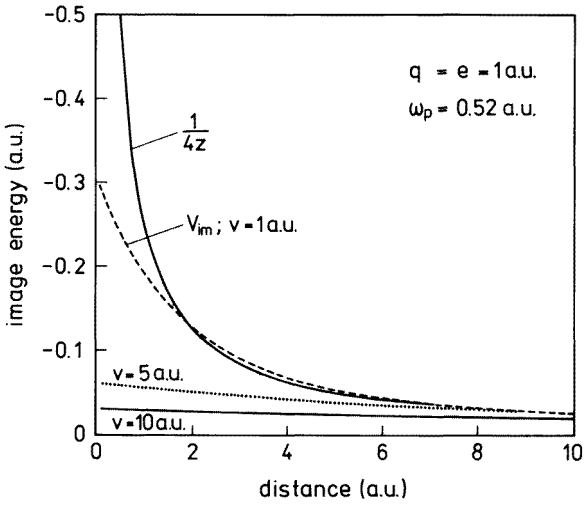

Figure 1. Image charge interaction energies as a function of the distance from the image reference plane for a particle with charge $q = e$ and a dielectric medium with $\omega_p = 0.52$ au (aluminium): ——, static limit $1/4z$; – – –, for a motion of the charge parallel to the surface with velocity $v = 1$ au derived from equation (1); · · · · · ·, $v = 5$ au; ——, $v = 10$ au.

projectile velocities $v_p < 1$ au, the simple classical expression will be a good approximation in most cases.

3. Trajectories of atomic projectiles in collisions with a solid surface

The trajectories of fast atomic projectiles with an initial (kinetic) energy E_0 for the scattering from a solid surface result from the atom–surface scattering potential. In general, this potential is described by a summation over all interatomic potentials between the projectile atom and individual atoms of the solid located at fixed positions $\boldsymbol{r}_i$ in the topmost surface layers. Then the scattering potential for the projectile at position $\boldsymbol{r}$ is $V_{surf}(\boldsymbol{r}) = \sum_i V(\boldsymbol{r}_i - \boldsymbol{r})$. The interatomic potentials V are described for collisions beyond the thermal regime by repulsive Coulomb potentials with a Thomas–Fermi type of screening, approximated by screening functions $\Phi(\boldsymbol{r}_i - \boldsymbol{r}) = \sum_k a_k \exp(-b_k|\boldsymbol{r}_i - \boldsymbol{r}|/a_s)$, where a_k and b_k are coefficients and a_s is a 'screening length' typically some tenths of an atomic unit of length $a_0 = 0.059$ nm (Ziegler *et al* 1985).

The surface plane defines a natural reference plane, so that it is favourable to describe trajectories and motion of projectiles during the scattering event with the solid in components of coordinates normal (z axis) and parallel (x–y plane, here denoted by the index p) with respect to the surface plane. Then the motion of projectiles (mass M) in the collision with the surface is given by the energy relation

$$E(\boldsymbol{r}(t)) = \tfrac{1}{2}Mv_p^2 + \tfrac{1}{2}Mv_z^2 + E_{im}(z) + V_{surf}(\boldsymbol{r}) - E_{diss}(\boldsymbol{r}) \qquad (2)$$

where E_{diss} is the dissipation of energy in the collision via transfer of energy to the target (electronic excitations, etc). The initial energy of the projectiles is $E_0 = E(\boldsymbol{r}(-\infty)) = \tfrac{1}{2}Mv_0^2 = \tfrac{1}{2}M(v_{0,p}^2 + v_{0,z}^2)$ for a 'macroscopic' incidence angle (determined by the geometrical adjustment of the projectile beam relative to the surface plane) $\Phi_{in} = \tan^{-1}(v_{0,z}/v_{0,p})$. We

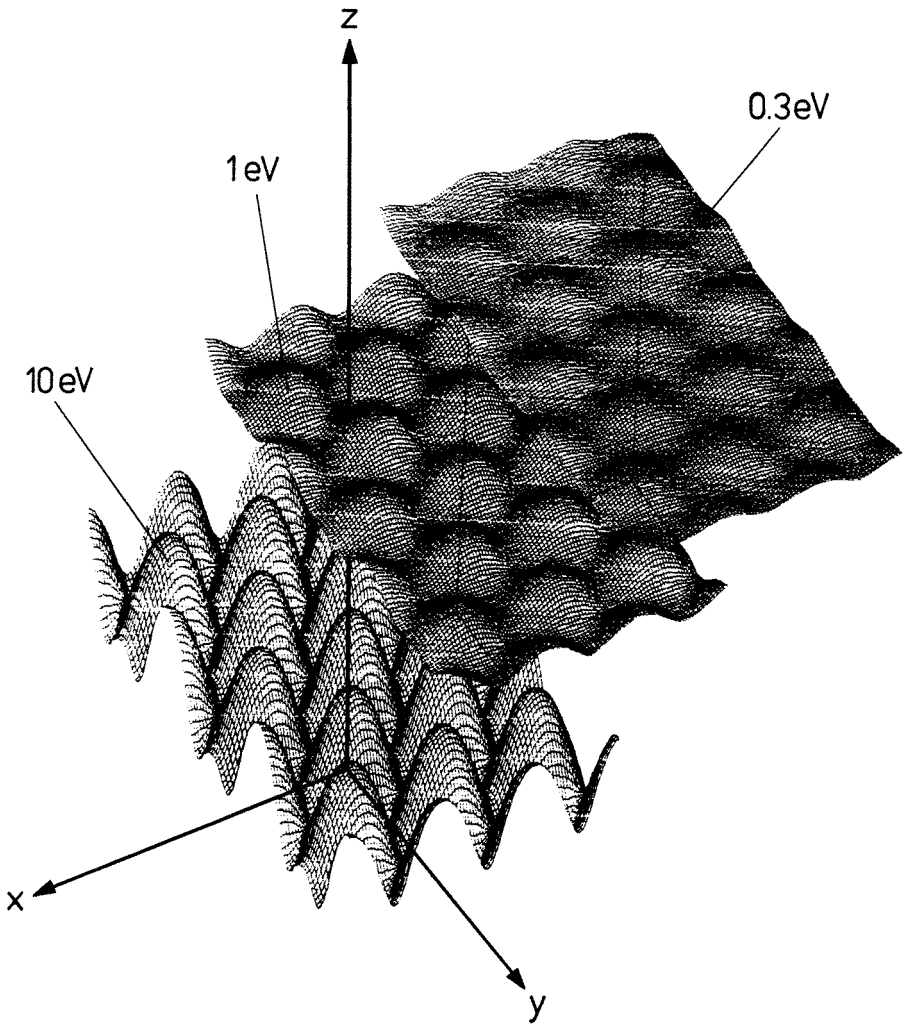

Figure 2. Equipotential planes of the scattering potential for K atoms in front of an Al(111) surface.

then have

$$E_{0,p} = E_0 \cos^2 \Phi_{in} \qquad E_{0,z} = E_0 \sin^2 \Phi_{in} \tag{3}$$

for the initial kinetic energies for the motion parallel and normal to the surface plane. The ratio of E_p to E_z can be adjusted over a wide range via setting the incidence angle Φ_{in}.

Close to the surface the initial straight-line trajectories are predominantly modified by the atom–surface potential V_{surf}. In figure 2 we show equipotential planes of this potential for K atoms in front of an Al(111) surface for 0.3, 1, and 10 eV, respectively (Nienhaus 1988). An increased corrugation of the potential with increasing energy is evident, and for higher potential energies than shown here the potential surfaces start to 'leak' between the atomic cores of the topmost layer.

The effect of the corrugation on projectile trajectories is illustrated for 10 eV Na

atoms scattered at $\Phi_{in} = 45^\circ$ from a Cu(100) surface along the $\langle 100 \rangle$ direction. Figure 3 shows calculated trajectories in a plane normal to the surface, where a broadening of the scattered beam over a wide angular range is apparent (Cooper and Behringer 1994). In these calculations, E_{im} and also E_{diss} are neglected so that the initial energy E_0 is conserved. However, owing to the corrugated structure of the scattering potential this conservation does not hold for the separated parallel and transverse motion. This means that a coupling between perpendicular and parallel motion is effective and $v_z(t = -\infty) \neq v_z(t = \infty)$ and $v_p(t = -\infty) \neq v_p(t = \infty)$.

The effect of the corrugation of V_{surf} on the angular spread of trajectories can be reduced for collisions with decreasing Φ_{in}, since the projectiles probe an increasing portion of the potential surface instead of domains around single target atoms. This feature is demonstrated in figure 4 for 1 keV Ar projectiles scattered from a row of Al atoms. The trajectories for a larger Φ_{in} show a pronounced angular spread, whereas for a smaller Φ_{in} a 'specular reflection' for the projectiles is observed, i.e. all projectiles are scattered with nearly identical trajectories. This is the regime of *surface scattering at a grazing angle of incidence.*

For grazing incidence, collisions with the surface proceed under 'channelling' conditions (Gemmell 1974) where the effective scattering potential results from an averaging of $V_{surf}(\boldsymbol{r})$ over the positions of the surface atoms and depends on the distance from the surface only:

$$U(z) = \langle V_{surf}(\boldsymbol{r}) \rangle_{surface\ atoms}. \tag{4}$$

'Critical energies' with respect to the validity of the channelling concept amount from typically some 10 eV for light atoms up to some 100 eV for heavy collision partners. Under ideal channelling conditions (we restrict our discussions here to 'planar channelling', i.e. the scattering proceeds at random to a low indexed direction in the surface plane) the parallel motion and normal motion of the projectiles are decoupled completely, and energy conservation holds for both components (energy losses neglected). Then, for grazing scattering, equation (2) can be decomposed according to

$$E_p = E_0 \cos^2 \Phi_{in} = \tfrac{1}{2} M v_{0,p}^2 \tag{5}$$

$$E_z = E_0 \sin^2 \Phi_{in} = \tfrac{1}{2} M v_z^2(\boldsymbol{r}) + U(z) + E_{im}(z) \tag{6}$$

so that during the collision the projectile beam forms the angle $\Phi(\boldsymbol{r}) = \tan^{-1}(v_z(\boldsymbol{r})/v_{0,p})$ with the surface plane. Experiments in grazing scattering geometry are performed at incidence angles Φ_{in} ranging from less than 0.1° to some degrees, so that E_z is three to six orders of magnitude smaller than $E_p \cong E_0$. Then, even for projectiles with kiloelectronvolt or megaelectronvolt energies, E_z will be in the electronvolt domain. These two vastly different energy regimes for scattering with the solid have interesting new features in the study of atom–surface interations as shown below.

The effective potential energy $U_{eff}(z) = U(z) + E_{im}(z)$ for the normal motion is shown in figure 5 for a proton in front of an Al(111) surface. $U(z)$ is derived here from a screened Coulomb potential as given by Ziegler *et al* (1985). Note that, owing to the attractive and long-ranged image potential, U_{eff} shows a minimum. The distance z_{min} of closest approach to the surface plane is slightly affected by E_{im} and amounts to about 2 au for an E_z of some electronvolts. Furthermore we see from the figure that $U(z)$ is of relatively short range in comparison with the image potential and distances relevant for charge exchange phenomena (the image potential plotted in figure 5 is assumed to saturate below $z - z_{im} \approx 4$ au owing to charge exchange).

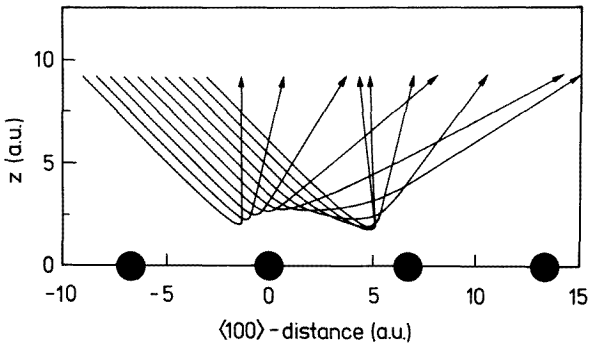

Figure 3. Trajectories of 10 eV Na atoms scattered from Cu(100) along the ⟨100⟩ direction (Cooper and Behringer 1994).

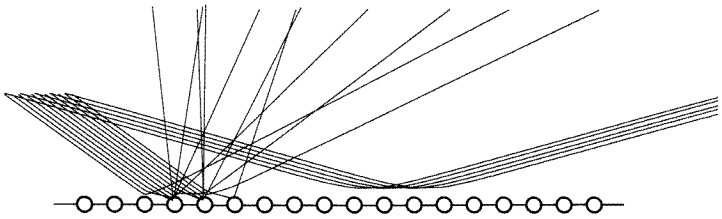

Figure 4. Trajectories of 1 keV Ar atoms scattered from Al(111) along the ⟨110⟩ direction.

4. Study of charge exchange in ion surface scattering

In recent years, considerable progress has been achieved in the detailed understanding of charge exchange processes of atoms in front of metal surfaces. This holds in particular for the resonant electron transfer and the incorporation of kinematic effects in theoretical treatments. As a representative example we shall discuss the neutralization of fast Na^+ ions during grazing scattering from an Al(111) surface. Whereas gross features of alkali-atom interactions with metal surfaces are well established 'surface ionization', etc (see, e.g., Kaminski (1965)), important details on charge exchange have been worked out over the last few years.

In figure 6 we show the neutral fraction P_0 as a function of projectile velocity after the scattering of fast Na^+ ions from an Al(111) surface at a grazing incidence angle Φ_{in} of about 1°. Φ_{in} is adjusted in such a manner that the normal velocity component is kept constant ($v_z = 2.65 \times 10^{-3}$ au). The data show a monotonic decrease with increasing velocity which can simply be understood by a kinematic effect. Energies of electronic states of a metal forming the conduction band appear in the rest frame of the moving atom modified (Galilei transformation) so that the clear-cut separation of occupied and empty metal states at the Fermi level is abandoned. Then the occupation of metal states is given by a 'Doppler–Fermi–Dirac distribution' (Newns 1989, Los and Geerlings 1990), and the kinematically induced resonances with unoccupied metal states result in the experimentally observed decay of P_0.

The solid curve in figure 6 is the result of parameter-free calculations (Borisov *et al* 1996a, b) which reproduce the data on a quantitative level. The theory is based on a master

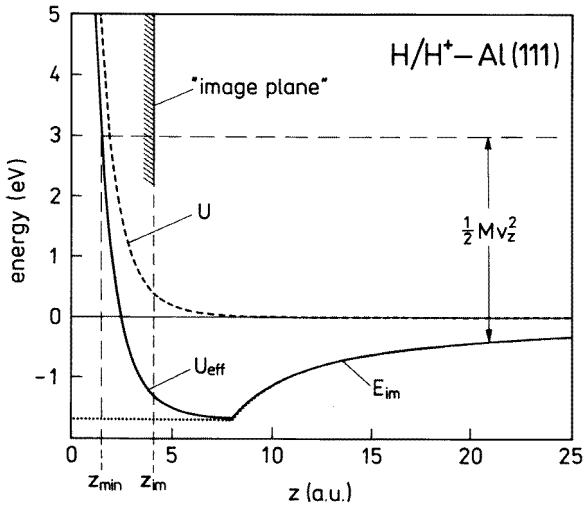

Figure 5. Planar channelling potential energies for H/H^+–Al(111) scattering with respect to the transverse motion.

equation for the occupations of the atoms in the neutral and ionized charge states (N_0 and N^+, respectively) for charge exchange via resonant one-electron tunnelling (Zimny *et al* 1989):

$$\frac{dN_0}{dt} = -g_l\Gamma_l N_0 + g_c\Gamma_c N_+. \tag{7}$$

The rate equation approach has been shown to hold for grazing ion–surface collisions (Geerlings *et al* 1986). For an Al(111) surface (work function $W = 4.3$ eV), populations different from the ground-state terms of the neutral atom and the Na^+ ion can be neglected, so that the normalization is $N_0 + N_+ = 1$. $g_l = 1$ and $g_c = 2$ are spin-statistical factors for electron loss and capture; Γ_l and Γ_c are electron loss and capture rates obtained from a non-perturbative scattering method (Nordlander and Tully 1989, Borisov *et al* 1996a, b). These rates and the total transition rate $\Gamma = \Gamma_l + \Gamma_c$ show to a good approximation an exponential decay with the atom–surface separation as demonstrated in the upper part of figure 7. Close to the surface, i.e. in the apex of the trajectory, rates are sufficiently large that the interplay of electron loss and capture events in equation (7) leads to an equilibrium of the atomic occupation determined by the ratio of loss rate to capture rate. Any 'memory' of the initial occupation is erased for grazing scattering, where normal velocities v_z are generally less than 0.1 au.

The final formation of atomic populations takes place on the outgoing path around a distance z_s, where the transition rates are sufficiently small to provide a survival from further electronic transitions and to 'freeze' the transient charge state (Overbosch *et al* 1980). The solution of equation (7) with respect to the final atomic occupation can be written as

$$P_0(\infty) = \int_{traj} dz\, P_a^{eq}(z) F(z) \tag{8}$$

where the equilibrium population P_a^{eq} shows only a weak dependence on z. Thus the distribution function $F(z)$ (shown for Na–Al in the lower part of figure 7) determines the effective range of distances for charge exchange. $F(z)$ is a peaked function that is non-zero

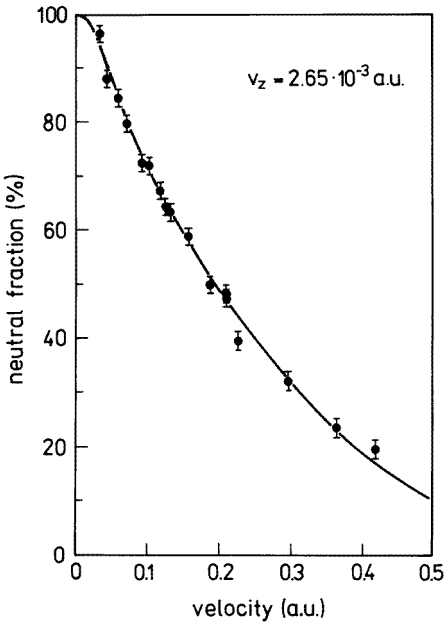

Figure 6. Neutral fractions as a function of projectile velocity after the scattering of Na^+ ions from Al(111), where the normal velocity component is kept constant at $v_z = 2.65 \times 10^{-3}$ au: ——, calculations based on transition rates obtained with the CAM method (see text).

within a defined interval of distances with a maximum at z_s. For a transition rate described by a single exponential $\Gamma(z) = \Gamma(0)\exp(-z/z_c)$, z_s can be deduced from $z_s = z_c \ln(\Gamma(0)z_c/v_z)$ (Hagstrum 1954, Overbosch *et al* 1980), i.e. z_s shows a slight dependence on the normal velocity component v_z as can be seen from the two functions displayed for 0.002 and 0.004 au ($E_z = 2.3$ and 9.2 eV).

4.1. Image charge effects on the outgoing trajectory: formation of Na atoms

The existence of a 'freezing distance' in atom–surface interactions follows from measurements of charge state distributions in an indirect manner only. From our discussion outlined above, however, it is evident that image charge effects provide specific information in this respect. The effects of charge exchange and image charge on the outgoing trajectory for neutral atoms and ions are sketched in figure 8. At distances $z < z_s$, electron loss and capture affect the charge state of the projectiles whereas, for $z > z_s$, the projectiles will keep the charge state defined in the interval around z_s. Then atoms will be neutral on the further outgoing path, and ions keep their charge. On the remaining path, ions are attracted via image forces towards the surface, so that charged particles emerge at smaller scattering angles than neutral particles do. Since the energy for the normal motion of ions is reduced because of image charge interaction on the outgoing trajectory starting from z_s to infinity, i.e. $E_{im}(z_s) = 1/4z_s$, one can deduce from E_{im} the distance z_s of final formation.

E_{im} is obtained from measurements of angular distributions separated with respect to outgoing atoms and ions. From the exit angles Φ^0_{out} and Φ^+_{out} and the normal energies $E^0_z = E_0(\Phi^0_{out})^2$ and $E^+_z = E_0(\Phi^+_{out})^2 = E^0_z - E_{im}(z_s)$, we obtain $E_{im}(z_s) = E_0[(\Phi^0_{out})^2 - (\Phi^+_{out})^2]$.

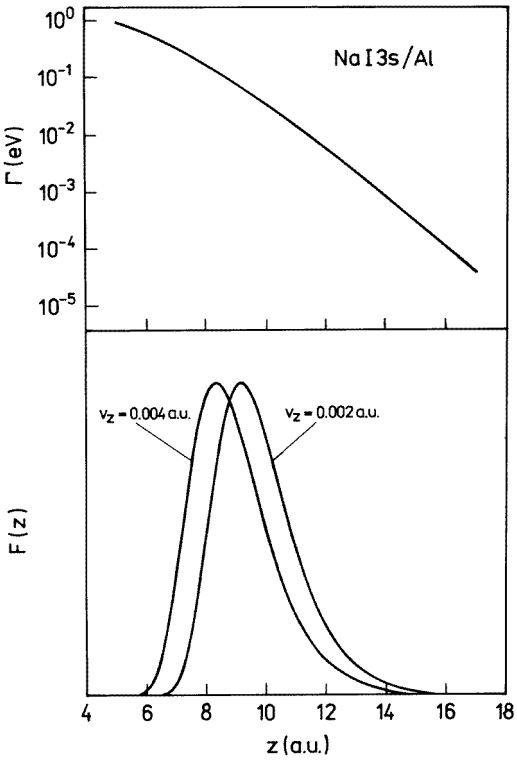

Figure 7. Total width Γ and distribution function $F(z)$ for resonant electron transfer between NaI 3s and an Al surface. Note the dependence of the mean distance of formation on the transverse velocity component v_z.

For the angular shift between the two distributions we have (Winter 1992a)

$$\Delta\Phi_{out} = \Phi^0_{out} - \Phi^+_{out} \approx \Phi^0_{out}\left(1 - \sqrt{1 - \frac{E_{im}(z_s)}{E^0_z}}\right). \tag{9}$$

From this simple relation it is evident that sizable shifts can be achieved only if E_{im} is of the same order of magnitude as the normal energy E_z. Since $E_{im}(z_s)$ is typically in the electronvolt domain, it is advantageous to keep E_z of comparable magnitude. Thus experiments with fast projectiles have to be performed at grazing incidence, in order to make $E_z = E_0 \sin\Phi_{out}$ comparable with E_{im}.

For the formation of Na atoms and Na^+ ions, one obtains for 25 keV projectiles scattered with $\Phi_{out} = 0.9^\circ$ ($E^0_z = 6.2$ eV; $v^0_z = 3.3 \times 10^{-3}$ au) a mean final formation distance $z_s \approx 9$ au and $E_{im} = 1/4z_s = 0.75$ eV. (Note that, owing to van der Waals interaction, neutral atoms are also slightly attracted; this corresponds here to energies less than 0.1 eV (Borisov *et al* 1996a, Annett and Echenique 1986).) We then estimate from equation (9) a shift of only $\Delta\Phi_{out} = 0.048^\circ$.

In a series of studies we have shown that such small angular shifts can be detected experimentally. The essential prerequisite for those measurements are well defined conditions for the scattering process, i.e. very flat and clean single-crystal surfaces. By a large number of cycles of surface preparation via grazing-incidence sputtering with 25 keV Ar^+ ions and subsequent annealing, we finally obtained Al(111) surfaces free from

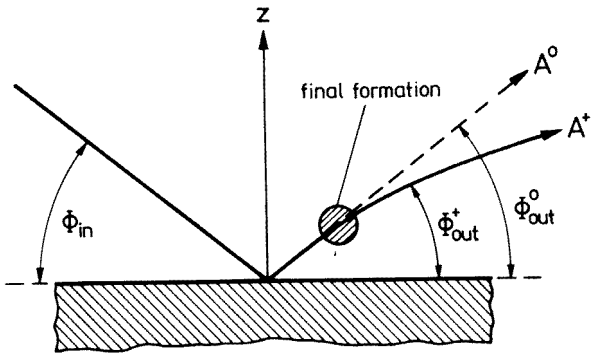

Figure 8. Sketch of image charge effects on the outgoing trajectory of an ion in grazing surface scattering.

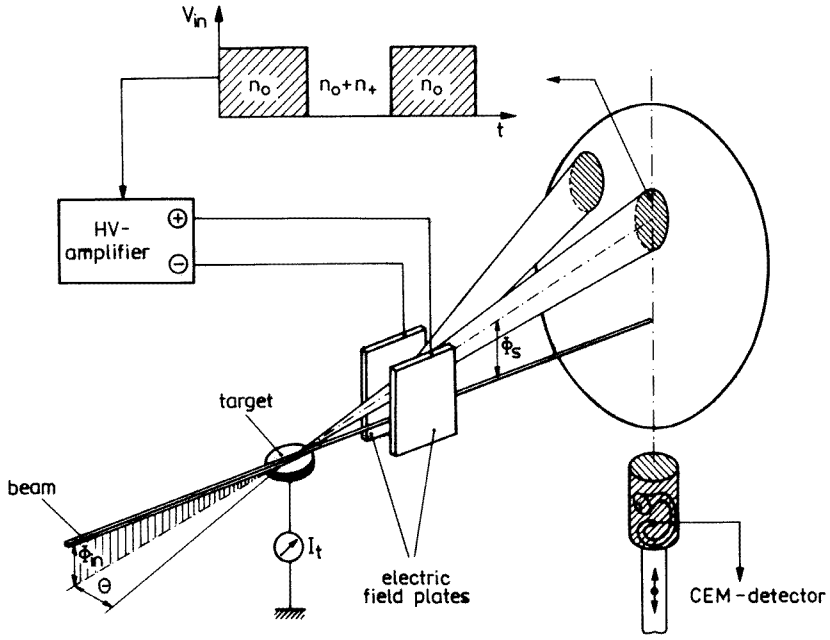

Figure 9. Sketch of the experimental set-up for measurements of angular distributions separated with respect to the charge state of the scattered projectiles.

adsorbates in the Auger spectroscopy detection limit and with terraces up to about 100 nm in width.

With such a surface we measure, with the set-up sketched in figure 9, well defined angular distributions, where separation of the data with respect to the charge states of the emerging projectiles is performed by the controlled application of an electric field via a 'difference method' as indicated in the figure. Angular distributions in the scattering plane are displayed in figure 10 as a function of Φ_{out} for emerging atoms (full circles) and ions (open circles). In order to demonstrate the small angular shift, both well defined distributions

(angular half-width $\delta\Phi \approx 0.25^\circ$) are normalized to the same heights of the maxima. A small but clearly resolved shift $\Delta\Phi = 0.4^\circ \pm 0.1^\circ$ between the peaks can be deduced in agreement with the estimate given above. Note that the shift between the two distributions decreases for larger Φ_{out}, since the normal energies E_z increase with increasing Φ_{out}^2 and image charge effects are reduced (see also equation (9)).

The size of the angular shift as well as the deflection of the ions towards smaller exit angles than for atoms is consistent with the concepts of charge exchange, in particular with the feature of relatively large and defined distances of final formation. Beyond this simple evaluation, we can obtain more detailed information from the data via a simulation procedure that incorporates the complete set of data. In this simulation we take the angular distribution for the neutral atoms as a reference for particles that are not affected by a direct image force. Then we compute with the distribution function $F(z)$ and the image potential the angular deflections of ions for each interval of a reference distribution. An illustration of the procedure is sketched for the data set presented later in figure 12.

The curves in figure 10 represent results of those simulations. The solid curve is obtained with rate parameters close to theory which reproduces the experimental data fairly well (the corresponding $F(z)$ is shown in the inset). In order to demonstrate the sensitivity of the angular deflection to the distance of formation, the rate is reduced by a factor of 50 so that $F(z)$ peaks at $z_s \approx 5$ au. Then the simulation (broken curves) shows a clearly larger angular deflection than observed. This can be considered as a direct signature that charge exchange proceeds at larger z_s here.

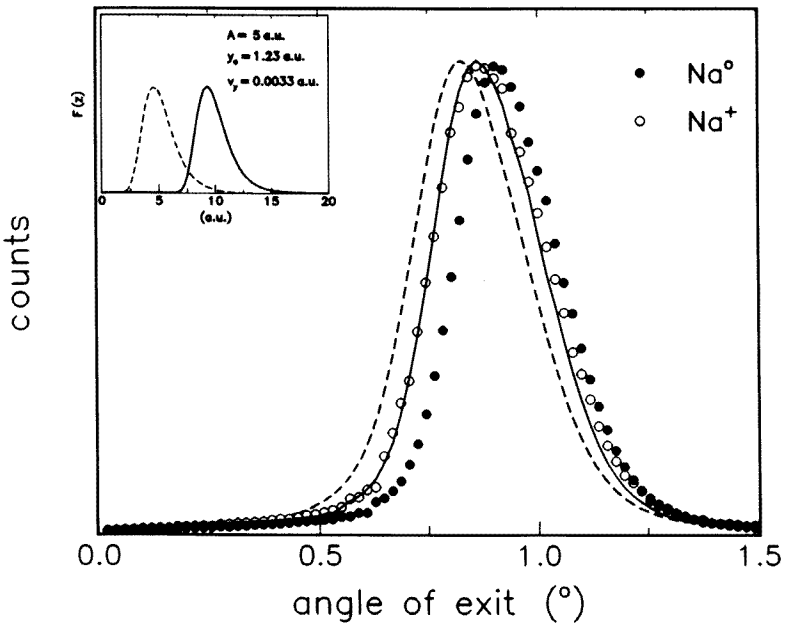

Figure 10. Angular distributions for Na atoms (●) and Na^+ ions (○) after the scattering of 25 keV Na^+ ions from Al(111): ——, – – –, results from simulations with the distribution function $F(z)$ for final formation as given in the inset. For details see text and figure 12.

For lower projectile energies image charge effects can also be observed by the modification of the projectile energy itself. In figure 11 we display energy spectra obtained

with a time-of-flight technique by Cooper and Behringer (1994) for the scattering of 23.8 eV Li^+ ions from a Cu(100) surface at $\Phi_{in} = \Phi_{out} = 35^\circ$. The data show peaked energy spectra where the distribution for ions is shifted to lower energies by about 0.9 eV in comparison with neutral atoms. This difference in energy can be ascribed to a loss on the outgoing path due to image forces acting on ions and thus amounts to $E_{im}(z_s)$. The observed effect is in close agreement with theoretical concepts of charge exchange; however, Cooper and Behringer (1994) stress that owing to 'experimental artefacts' (contact potentials, etc) the spectra should be interpreted only on a qualitative level.

4.2. Image charge effects on the outgoing trajectory: formation of hydrogen atoms

The neutralization of protons proceeds predominantly via the population of the 1s ground-state term of the hydrogen atom. Owing to the larger atomic binding energy of the 1s term ($E_a = -13.6$ eV) the decay length for resonant transition rates are smaller, so that the final formation of the atomic occupation proceeds closer to the surface. Furthermore, Auger capture and loss will play a role. This is, however, at present understood only on a qualitative level as discussed in a detailed paper by Zimny *et al* (1991). From resonant transfer transition rates published for hydrogen 1s in front of Al (Nordlander and Tully 1988) and estimates on Auger transition rates (Hentschke *et al* 1986), one deduces for grazing scattering of fast protons a final formation distance $z_s \approx 3$ au.

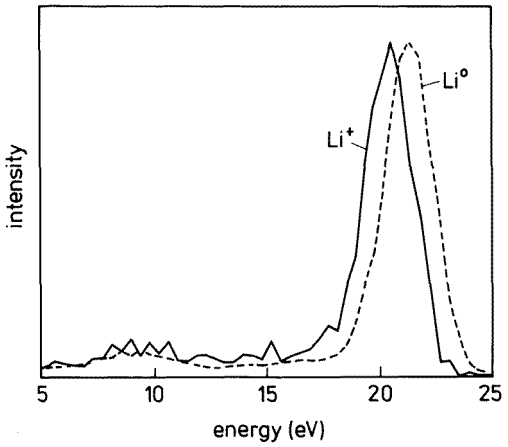

Figure 11. Energy spectra for neutral atoms and singly charged ions after the scattering of 23.8 eV Li^+ ions from Cu(100) along the ⟨100⟩ azimuth with $\Phi_{in} = \Phi_{out} = 35^\circ$. The intensities are normalized to same heights of the maxima. (From Cooper and Beheringer (1994).)

In figure 12 we present data obtained for the scattering of 25 keV protons from a Fe(110) surface (Winter and Leuker 1992). The angular distributions for atoms and ions show a pronounced shift which is clearly larger than observed for Na. This already indicates that the final formation has to proceed at smaller distances than about 8–10 au which is effective for Na atoms. The solid curve represents a simulation of the H^+ data with a distribution function $F(y)$ plotted in the inset. There are no calculations of transition rates available for this system. The analysis of data for the Fe target gives $z_s \approx 2.5$ au, which is the same size as estimated for Al.

For the H–Al system the angular distributions show angular shifts which are smaller

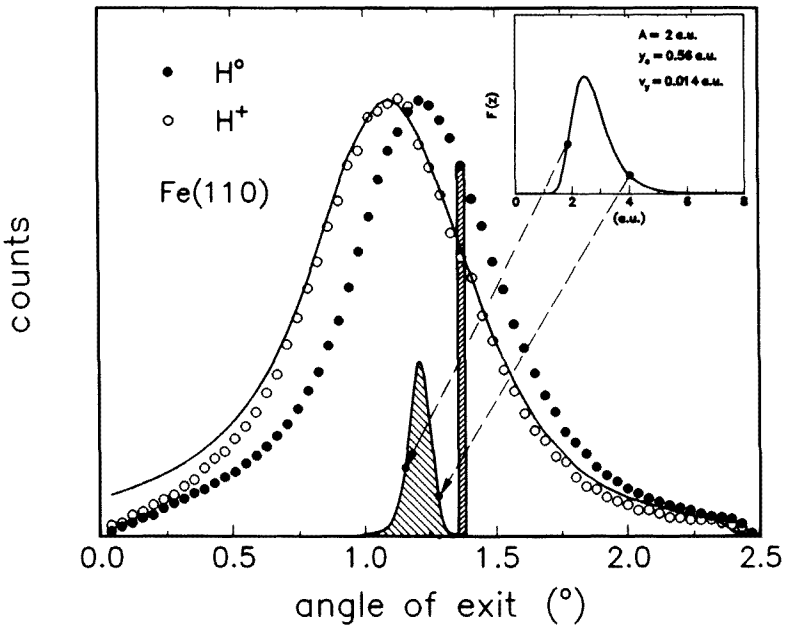

Figure 12. Angular distributions for H atoms (●) and protons (○) after the scattering of 25 keV protons from Fe(110). ——, represents the result of a simulation based on $F(z)$ as shown in the inset. The shaded areas illustrate the simulation procedure (see text).

than expected. This is demonstrated by data shown in figure 13 where the simulations give only reasonable agreement with the measurements for a function $F(z)$ peaking at $z_s \approx 6$ au instead of at the theoretically expected $z_s \approx 3$ au. This disagreement between experiment and theory is also apparent from the simple analysis of data by fits to Gaussian lineshapes which yield a shift of the maxima by $\Delta\Phi_{out} = 0.083^\circ$ equivalent to $E_{im} = 1.0$ eV. In a number of experiments performed with different Al targets and different set-ups we observed consistently image interaction energies $E_{im} = 1.0 \pm 0.15$ eV.

These energies clearly deviate from $E_{im} \approx 2.3$ eV as deduced from $1/4z_s$ for $z_s \approx 3$ au. In a recent paper by Winter and Borisov (1996) this discrepancy is analysed via a detailed theoretical study on the contributions of the resonant electron transfer channel. One finds that the resonant channel cannot explain the large distances z_s deduced from the experiments nor the charge fractions as functions of the projectile velocity. Thus we conclude that the neutralization of protons has to be dominated by the Auger processes and hope that this problem will stimulate calculations on the Auger channel with realistic atom–surface barriers. Recent work in this respect for the Auger neutralization of He^+ ions has indicated that the modelling of the potential barrier between the atom and the surface has a pronounced effect on Auger transition rates (Lorente *et al* 1994, Lorente 1995).

Interesting further aspects are the image charge phenomena at higher projectile energies. In figure 14 we show recent data obtained with 300 keV protons, where for a scattering angle $\Phi_s \approx 0.6^\circ$ ($\Phi_{in} \approx 0.3^\circ$) the normal energy is still in the electronvolt domain ($E_z \approx 8$ eV). Because of the very small angular shifts and the small neutral fractions of less than 1%, such experiments are difficult. However, an angular shift of $\Delta\Phi \approx 0.01^\circ$(!) could be unambiguously deduced from the data. This shift is equivalent to an image

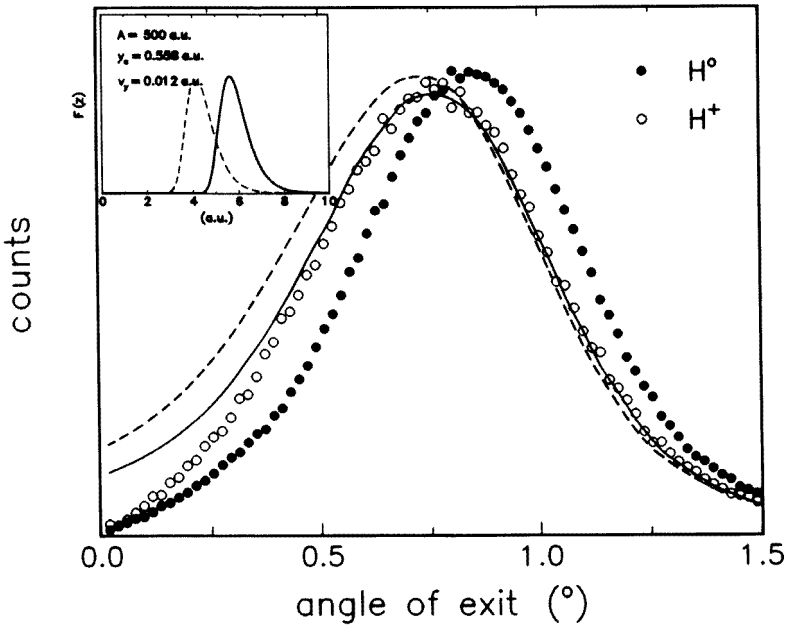

Figure 13. Same as figure 12, but for an Al(111) target.

energy $E_{im} \approx 0.5$ eV, less than observed for smaller projectile velocities. The chain curve represents a Gaussian lineshape with a shift $\Delta\Phi = 0.02^\circ$ which corresponds to $E_{im} = 1.0$ eV as measured at for example $E_0 = 25$ keV ($v_0 = 1$ au). The actual shift at $E_0 = 300$ keV ($v_0 = 3.5$ au) is undoubtedly smaller.

The reduced angular shift can be ascribed to retardation effects of the dynamical image potential at such high velocities (see figure 1). Since we do not expect that the total transition rates will strongly increase with increasing projectile velocity in this range, we have comparable 'freezing distances' z_s. Then experiments of this type provide dynamical tests of dielectric response theory (Nordlander 1992). Work on this problem is in progress (Winter 1996b).

4.3. Image charge effects on the incoming trajectory: scattering of hydrogen atoms and ions

In a similar way as on the outgoing path, trajectories of ions are also affected by image charge effects on the incoming part. However, the effects of the image charge are opposite in the two cases. On the incident trajectory, ions are accelerated and gain image energy, until the neutralization of the projectile ceases the attraction via image forces. It has been already shown by Hagstrum (1954) that, for electronic transition rates approximated by an exponential decay, first charge transfer is effective within a defined range from the surface. This results in a distance of survival from electron capture z_s, similar to the 'freezing distance' on the outgoing trajectory.

The gain in vertical energy increases the effective angle of incidence from $\Phi_{in}^0 = \tan^{-1}(E_{0,z}/E_{0,p})^{1/2}$ to $\Phi_{in}^q = \tan^{-1}((E_{0,z} + E_{im}^q)/E_{0,p})^{1/2} > \Phi_{in}^0$, where E_{im}^q is the image interaction energy of projectiles with charge q. Since the acceleration of the ions comes to

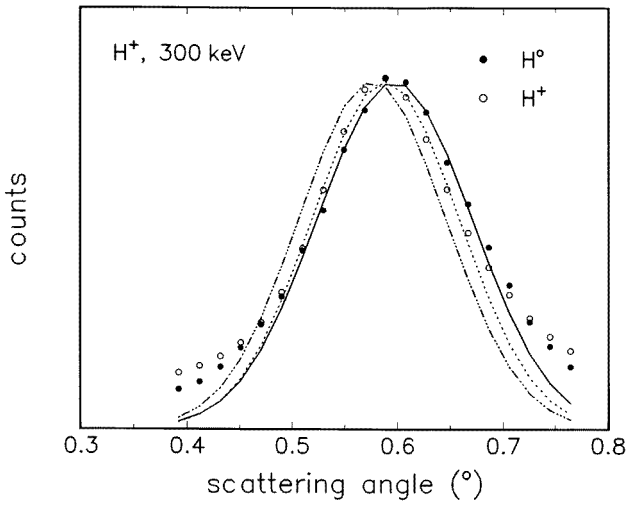

Figure 14. Angular distributions for H atoms (●) and protons (○) after the scattering of 300 keV protons ($v = 3.5$ au) from Al(111): fits to Gaussian lineshapes with an angular shift between both distributions of about 0.01°. — · —, an angular distribution which one would expect for comparable energy gains E_{im} as observed for lower velocities ($v \approx 1$ au).

an end before the surface scattering potential U sets in (see figure 5), ions are reflected at larger angles of incidence than neutral atoms are. For specular reflection, $\Phi^0_{in} = \Phi^0_{out}$ and $\Phi^q_{in} = \Phi^q_{out}$, so that incident ions are scattered at larger angles than atoms as sketched in figure 15.

This effect of the image charge is opposite to the deflection on the outgoing path. A further substantial difference is based on the feature that the charge state on the incident path is given by experimental settings, whereas on the exit the contributions of different charge states result from the dynamics of charge exchange between atom and surface. This feature is important for scattering experiments with multicharged ions (see below).

In figure 16 we show full angular distributions of 25 keV H^0 atoms and H^+ ions scattered from Al(111). By means of an electric field, only those projectiles are detected that leave the surface as neutral atoms (no image charge effects on outgoing trajectory). In contrast with the observation for the outgoing path (see figure 13), ions are scattered at larger scattering angles than atoms are, a signature of an attractive force on the incident trajectory. The angular shifts are comparable for both parts of the trajectory. This is demonstrated by a comparison of distributions for 'symmetric' scattering, i.e. H^+–H^+ and H^0–H^0, in figure 17. Image charge acceleration and deceleration on the incoming and outgoing paths, respectively, cancel each other, and the ions are scattered at the same angles as neutral atoms (no image forces). We conclude that the distances z_s for the onset of charge transfer and final formation are close to each other. Since charge transfer proceeds almost completely between conduction band states and the 1s ground-state term, this observation is consistent with theoretical concepts.

4.4. 'Skipping motion'

Specific features of charge exchange result for scattering of protons from Al(111) in interaction energies $E_{im}(z_s) \approx 1$ eV. For $E^0_z \rightarrow E_{im}(z_s)$ we find that $\Phi^+_{out} \rightarrow 0$ from

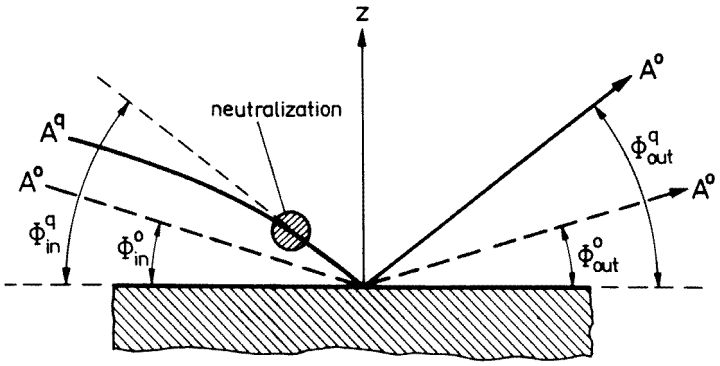

Figure 15. Sketch of image charge effects on the trajectory of an incoming ion with charge q.

equation (9), i.e. the ions are scattered parallel to the surface plane. A peculiar case is met for $E_{im}(z_s) > E_z^0$ since charged projectiles have insufficient transverse energies in order to overcome their image potential. Then fast ions are bound to the surface. In the static regime, this is the well established 'chemisorption', atoms are ionized close to the surface and trapped via image forces to the topmost layer of a solid (see, e.g., Lundqvist (1986)).

'Skipping motion', a hopping of fast ions on the surface, has been proposed by Ohtsuki *et al* (1979). The basic concepts for describing skipping phenomena are outlined in figure 18. In figure 18(a) we display a scattering potential U_{eff} as discussed in figure 5. Ions can be bound in the potential well formed for negative potential energies, when the incoming projectile loses transverse energy. In general, two different mechanisms are discussed for transitions to the skipping regime:

(1) Because of corrugation, imperfections, thermal vibrations of lattice atoms, etc, the scattering potential shows deviations from planar symmetry, and a coupling between normal momentum and parallel momentum is present, as indicated by the broadening of angular distributions. This reduction in the initial transverse energies leading to bound states (see also figure 3) has been investigated by Ohtsuki's group primarily via computer simulations (Ohtsuki 1983, Kato *et al* 1988, Sakai *et al* 1992, 1995) and is shown to be effective for projectiles with initial normal energies up to several electronvolts.

(2) Charge exchange plays an important role in skipping motion, since it affects the image charge interaction. The spread of the distances for first and final electron capture or loss leads to different potential curves, as sketched in figure 18(a) for two distances z_s. Then a trapping of projectiles can be described by a transition between two potential curves for $z_s^{in} > z_s^{out}$ (Winter *et al* 1992). Since for protons on Al(111) we have $E_{im}(z_s) \approx 1$ eV, this mechanism is predominantly effective for initial normal energies in the subelectronvolt domain. Note that, in particular, neutral incident projectiles without image charge attraction (corresponds to large z_s^{in} in the figure) will most preferentially be trapped via a transition to an ionic potential curve. This mechanism also leads to a broadening of scattered beams (Kato and Snowdon 1994).

In figure 18(a) we show in addition the case, where a projectile overcomes the scattering potential and penetrates the topmost layer of the surface. Then the particle is bound between the two planes of the topmost and second surface layer and performs a so-called 'subsurface channelling', a motion well established for trajectories of swift ions in the bulk of thin single-crystal foils (Gemmell 1974, Lutz *et al* 1966, Eisen and Robinson 1971). The projectiles

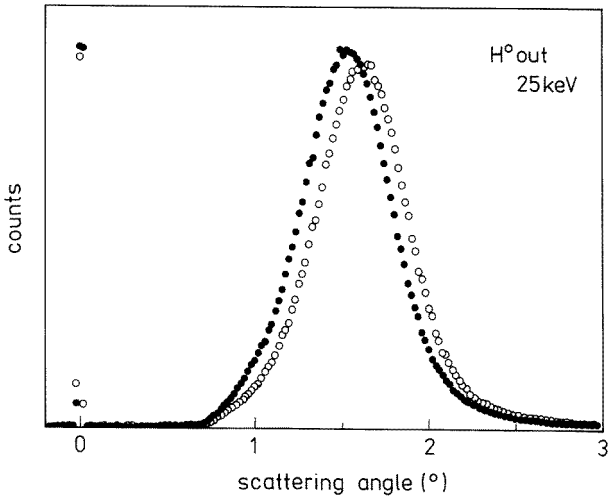

Figure 16. Angular distributions for neutral H atoms after the scattering of 25 keV H atoms (●) and protons (○) from Al(111). The data are arbitrarily normalized to the same heights of the peaks.

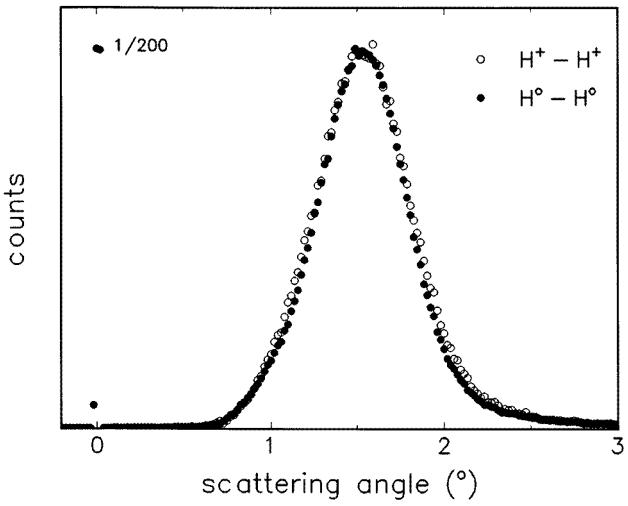

Figure 17. Angular distributions for 25 keV incident and outgoing protons (○) and for atoms (●).

are assumed to penetrate the surface owing to imperfections (e.g. steps) or owing to thermal vibrations of lattice atoms (Sakai *et al* 1992). In this respect it is favourable for the projectiles to have relatively large normal energies, in contrast with the condition required to enter the skipping regime.

Typical trajectories for 'skipping motion' (labelled B) and 'subsurface channelling' (labelled C) are sketched in figure 18(b) (note the different length scales for the parallel and normal component). From the simple sketch of trajectories we deduce a signature for the different types of trajectory. A regularly scattered projectile (A) will undergo a mean

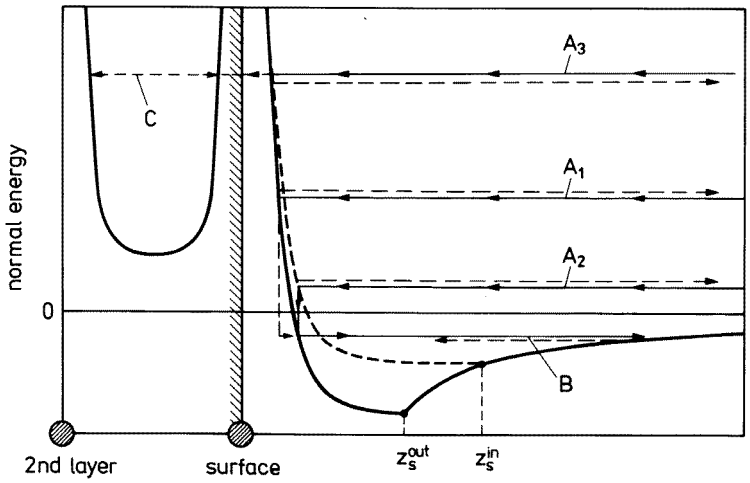

(a)

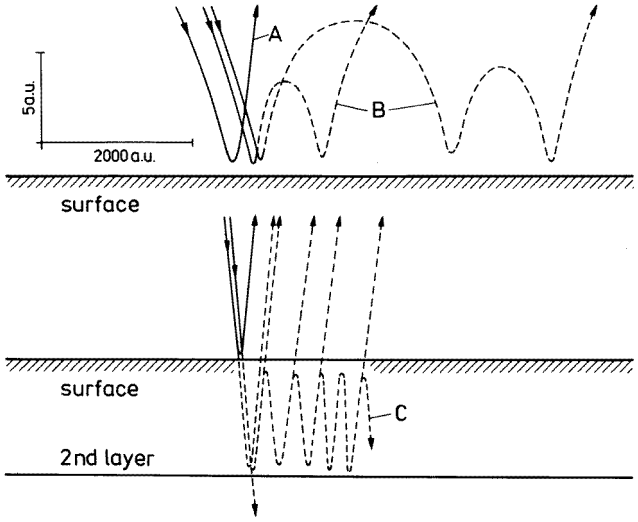

(b)

Figure 18. (a) Scattering potentials for the transverse motion of neutralized ions and reionized atoms in front of a metal surface. A_1 and A_2 denote cases that might perform transitions to a bound motion (B); A_3 might go over to 'subsurface channelling' (C). (b) Trajectories resulting from the potentials and the transitions shown in (a): A, specular reflection; B, 'skipping motion'; C, 'subsurface channelling'. (Trajectories from Sakai *et al* (1992).)

energy loss ΔE in the collision with the surface. Most of this energy is dissipated in the close vicinity of the surface, since here the density of conduction electrons is clearly larger than for distances beyond the jellium edge or image plane. Then projectiles performing a 'skipping motion' will show energy losses of the kind $\Delta E_n \approx n\ \Delta E$, where n is the number of collisions with the surface. From this property, evidence for skipping motion can be obtained in an experiment by the presence of discrete structures in energy loss spectra for scattered projectiles.

Subsurface channelling is also expected to show discrete energy losses. Since the projectiles are reflected an odd number of times between two crystallographic planes, one expects energy losses $\Delta E_n \approx (2n-1)\ \Delta E$. Thus, despite the fact that 'skipping motion' and subsurface channelling both show discrete energy losses, the two processes can be separated in the experiments. The clear-cut separation may, however, be less pronounced than expected from simple considerations, since for example the energy losses for kiloelectronvolt protons depend on angle and energy (Stölzle and Pfandzelter 1992, Wilke 1994) and may differ also for trajectories within and outside the bulk of the solid.

Finally we point out, that the projectile motion bound to the surface or to a planar channel can only be detected after the particles have left these regimes. The mechanisms that will excite the projectiles to an unbound motion again can be considered as similar to those that trigger transitions to bound states but operate in the reverse way.

4.5. Experimental evidence for 'skipping motion'

In the previous section it is argued that evidence for 'skipping motion' can be obtained experimentally via multiple discrete energy losses of scattered projectiles. A conceptual problem in experimental studies is based on the feature that projectiles which undergo 'subsurface channelling' will show similar energy loss structures. The partly controversial discussions and interpretations of experiments showing evidence for 'skipping motion' are caused by this ambiguity. However, the experiments performed so far indicate that the two different regimes of bound motion can be separated. Thus there is convincing evidence for 'skipping motion' observed by a number of groups in detailed energy loss studies.

First observations of discrete multiple energy losses in grazing ion–surface scattering have been reported by Kimura *et al* (1987) for He^+ ions scattered with energies of about 1 MeV from a SnTe surface. The high normal energy of the incident beam of $E_z \approx 20$ eV and energy losses scaling as $\Delta E_n/\Delta E_1 \approx 1{:}3{:}5$ are clear indications for subsurface channelling between atomic planes below the surface. 'Skipping motion' has been explicitly ruled out by these workers.

For projectiles with much lower energies, Si^+ ions with kiloelectronvolt energies scattered from Cu(111), Snowdon *et al* (1988, 1989) observed discrete structures in their energy loss spectra and ascribed their observations to 'skipping motion' or 'transient adsorption'. However, from the discussions given above, most of these observations can hardly be understood as signatures of skipping trajectories. Some items of criticism in this respect are

(1) that the discrete energy losses show a scaling closer to $\Delta E_n/(E_l \approx 1{:}3{:}5$ rather than to 1:2:3,

(2) (partly very pronounced) discrete structures in the energy are apparent in the data up to normal incident energies of several tens of electronvolts and for Si^- ions even 100 eV and

(3) the structures are even prominent with a target in an early state of preparation, i.e. a surface with a higher density of defect structures.

Thus one is tempted to state that these observations are consistent with subsurface channelling. These early studies gave a strong impetus to research in the field and initiated further work on the experimental verification of 'skipping motion'.

Detailed energy loss studies of fast protons scattered from a highly oriented polycrystalline graphite (HOPG) surface have been reported by Stölzle and Pfandzelter (1990, 1991, 1992). In figure 19 we display spectra obtained for 31.7 keV protons for angles

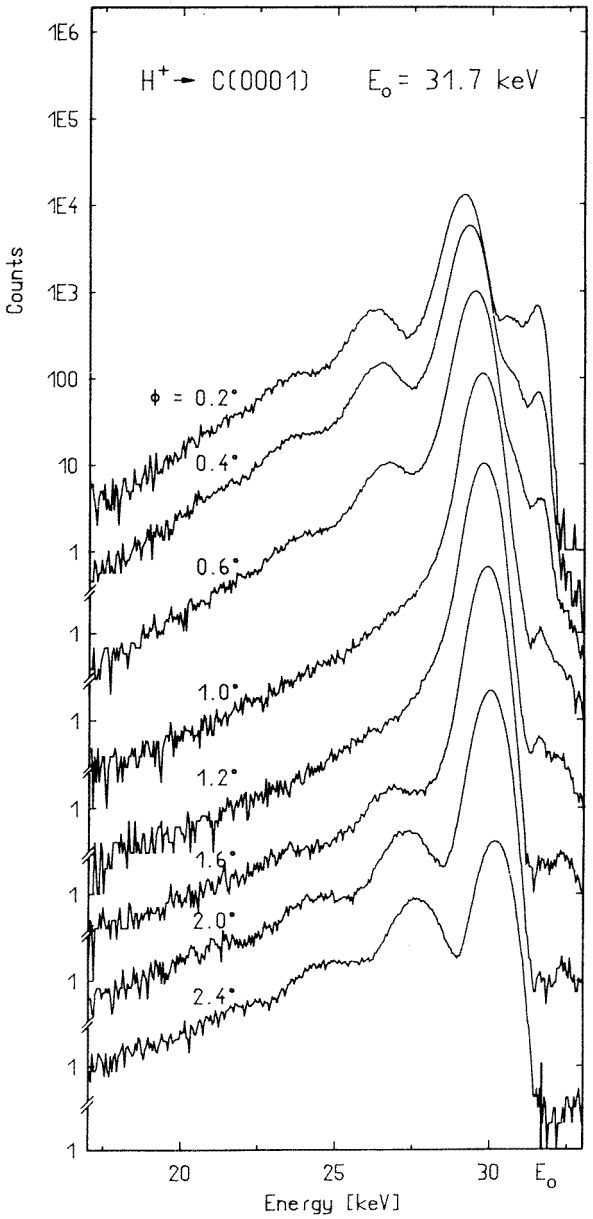

Figure 19. Energy spectra of 31.7 keV protons scattered under specular conditions from C(0001) for different incidence angles $\Phi_{in} = \Phi$. (From Stölzle and Pfandzelter (1991).)

of incidence from $\Phi_{in} = 0.2^\circ$ to 2.4° and detection under specular conditions ($\Phi_{out} \approx \Phi_{in}$). The spectra for small Φ (small E_z) show discrete energy loss structures; here E_z is less and can be up to some electronvolts. With increasing Φ the structures disappear for $\Phi \approx 1^\circ$ ($E_z \approx 10$ eV) and show up again for larger angles with more pronounced structures than for small Φ. These data can be consistently interpreted as the observation of a transition

from 'skipping motion' at small Φ to subsurface channelling at larger Φ. In this respect some specific items have to be noted.

(1) The data show the expected ΔE_n scalings for the two regimes, although somewhat obscured, since the mean energy loss decreases with increasing Φ and decreasing energy (Stölzle and Pfandzelter 1992).

(2) The normal energies $E_z \approx 10$ eV ($\Phi_{in} \approx 1^\circ$) where structures due to skipping motion are washed out ('critical energy' for 'skipping motion') appear somewhat too large for a transition to a bound motion, but the mosaicity of the target may provide the scattering potential for an efficient normal conversion of transverse energies.

(3) An additional weak structure at low energy losses is attributed to binary collisions with atoms forming surface defects or with adsorbed atoms.

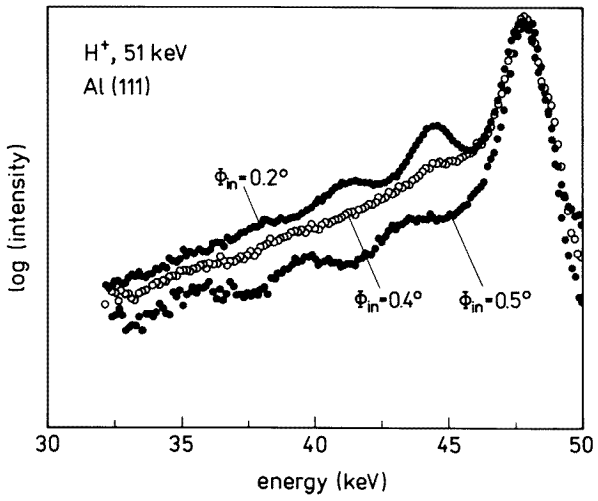

Figure 20. Energy spectra of 51 keV protons scattered from an Al(111) surface at $\Phi_{in} = \Phi_{out} = 0.2^\circ$, 0.4° and 0.5°.

Since the primary energy loss is found to be independent of angle and energy for protons scattered at medium energies from Al(111), this is a favourable system for isolating 'skipping motion' in an experiment. In figure 20 we show spectra for 51 keV protons scattered from Al(111) at $\Phi_{in} = 0.2^\circ$, 0.4° and 0.5° (Sommer 1991, Winter and Sommer 1992), i.e. $E_z = 0.6$, 2.4 and 3.9 eV. In a similar way to the graphite target, the data indicate a transition from skipping to subsurface motion. For $\Phi_{in} = 0.2^\circ$, the energy losses scale according to $\Delta E_n/\Delta E_l \approx 1{:}2{:}3$ and, for $\Phi_{in} = 0.5^\circ$, $\Delta E_n/\Delta E_l \approx 1{:}2.6{:}3.8{:}5$. Note that for smaller Φ_{in} the intensity for the multiple loss structures is clearly higher.

For the detection of the bound motion at the surface the projectiles have to leave this regime. This aspect has been investigated by Wilke (1994) via energy loss spectra for fixed incidence angles Φ_{in}. In figure 21, typical results for 25.1 keV protons scattered from Al(111) at $\Phi_{in} = 0.32^\circ$ and 0.82° indicate that for the smaller initial transverse energy ($E_z = 0.8$ eV) the structures in the spectra are prominent for specular and, in particular, for subspecular detection. For $\Phi_{in} = 0.82^\circ$ ($E_z = 5.1$ eV) the structures are prominent for specular and overspecular detection and disappear for subspecular angles. This observation is in agreement with the consideration that only small normal energies are needed to leave

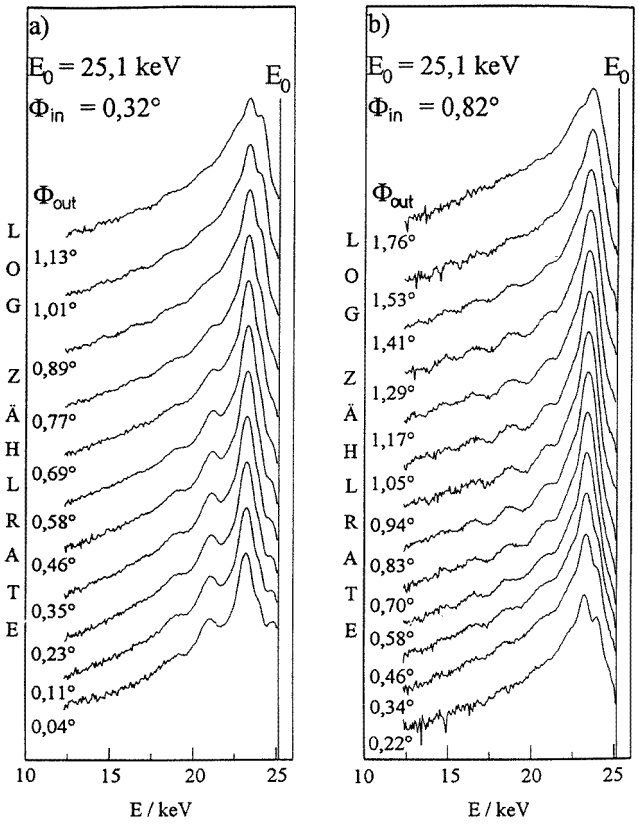

Figure 21. Energy spectra of 25.1 keV protons scattered from an Al(111) surface at $\Phi_{in} = 0.32^\circ$ (left part) and 0.82° (right part) as a function of Φ_{out}. (From Wilke (1994).)

the weakly bound state of skipping, whereas rather violent collisions are needed to overcome the higher binding energies in subsurface channelling.

As a consequence, the two mechanisms resulting in multiple discrete energy loss structures can be separated experimentally. Different behaviour is also evident in loss spectra recorded with a clean target (solid curves in figure 22) and a target with an enhanced number of defects of the surface structure after grazing sputtering (broken curves). The data obtained by Wilke (1994) with 20.1 keV protons show for $\Phi_{in} = 0.25^\circ$ ($E_z = 0.4$ eV) a vanishing multiple loss structure for the target of poorer quality, whereas for $\Phi_{in} = 0.91^\circ$ ($E_z = 5.1$ eV) the damped oscillatory structure is well preserved and enhanced in intensity. At small Φ_{in} we have 'skipping motion' in front of the surface plane, distorted by any kind of defect of the surface structure. Subsurface channelling proceeds in the first layers of the bulk of the crystal and will be less affected by defects in the surface region. Furthermore, higher densities of defects and adatoms at the surface will enhance contributions of binary collisions and the chance to penetrate the surface layer to enter subsurface channelling.

Discrete energy loss spectra have also been observed for the scattering of protons from the surface of an insulator (KCl) by Narumi *et al* (1994a). Here the dielectric function $\varepsilon(\omega)$ leads to an image potential derived from equation (1) that is about 50% smaller than for metals. Equal energy spacings in the spectra of $\Delta E \approx 2$ keV are observed, i.e.

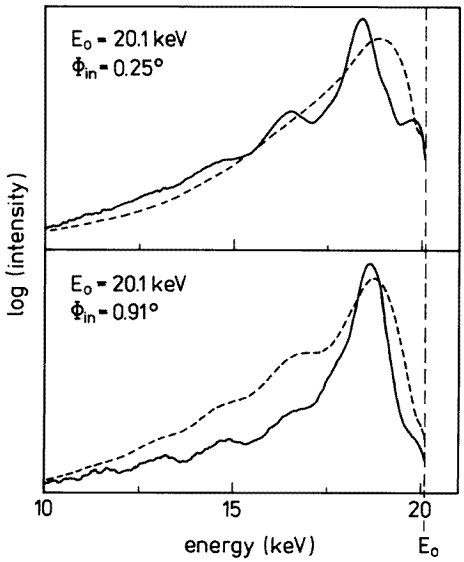

Figure 22. Energy spectra of 20.1 keV protons scattered at $\Phi_{in} \approx 0.25^\circ$ (upper part) and $\Phi_{in} = 0.91^\circ$ (lower part) from an Al(111) surface after preparation (——) and in an early state of preparation (– – –).

$\Delta E_n/\Delta E_l = 1{:}2{:}3$. Furthermore angular distributions for projectiles, which have undergone more than one discrete energy loss, do not depend on the incidence angle Φ_{in}. In figure 23 data are presented for $\Phi_{in} = 6.7$ mrad ($E_z = 1.3$ eV), $\Phi_{in} = 10.3$ mrad ($E_z = 3.2$ eV), and $\Phi_{in} = 13.4$ mrad ($E_z = 5.4$ eV). The arrows in the figure indicate the exit angles for specular reflection. The data show that any memory of initial transverse energies is lost, when projectiles are trapped in 'skipping motion'. Projectiles predominantly escape from this weakly bound motion with small transverse energies and are emitted under subspecular angles. Narumi *et al* (1994b) investigated also the effects of the roughness of the target surface on the energy loss spectra and observed similar data as discussed above for the Al(111) target.

The intensities of the discrete peaks in the spectra are also consistent with the expected behaviour for 'skipping motion'. The ratio of the intensity of the second peak to that of the first peak (see inset of figure) show a pronounced decay from about 1% at $\Phi_{in} = 6.7$ mrad to 0.1% at 13.4 mrad, which reflects the decreasing probability of entering the regime of 'skipping motion' for increasing transverse energies. On the other hand, the ratios of intensities of further subsequent peaks are found to be independent of Φ_{in}. This is also an indication for skipping, since projectiles with bound trajectories have made transitions to smaller transverse energies.

Additional important information is obtained from experiments with neutral projectiles. Neutral atoms are not affected by a direct image force on the incoming trajectory and do not gain additional transverse energy, i.e. the scattering potential U is effective here (broken curve in figure 5). Then of a given transverse energy E_z the probability of a transition to a bound motion of an ion is clearly higher than for incoming charged projectiles. In figure 24 we show energy spectra for the scattering of 30 keV protons and hydrogen atoms from an Al(111) surface at $\Phi_{in} = 0.2^\circ$ ($E_z = 0.4$ eV) and $\Phi_{out} = 0.15^\circ$. The two energy spectra indicate an increase in the relative intensity in the second loss peak by a factor of more

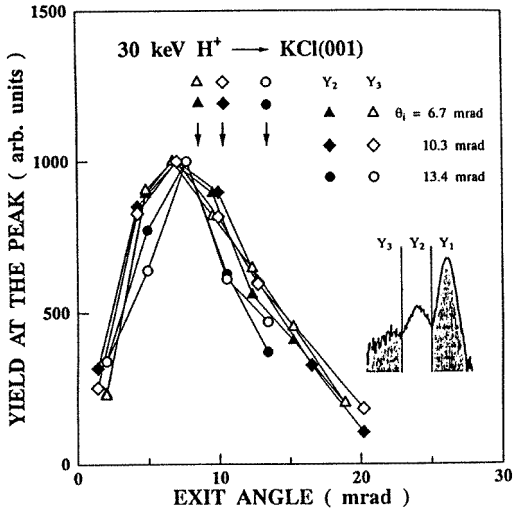

Figure 23. Angular distributions of the yields Y_2 and Y_3 (see inset) for the scattering of 30 keV protons from KCl(100).

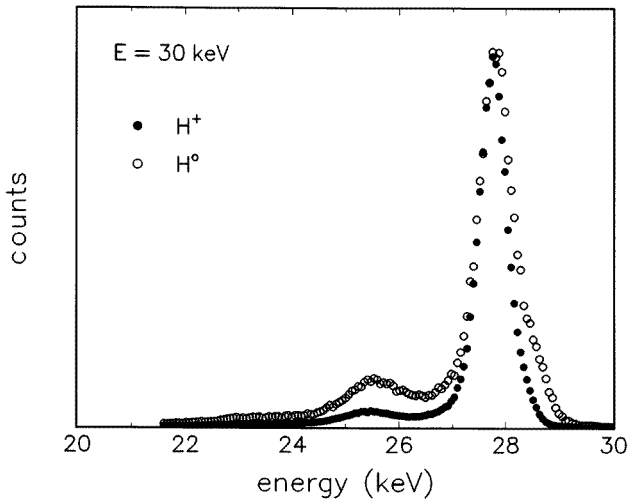

Figure 24. Energy spectra for 30 keV projectiles (● , protons; ○ , H atoms) after scattering from Al(111) at $\Phi_{in} = 0.2^\circ$ and $\Phi_{out} = 0.15^\circ$. The data are presented on linear scales and are arbitrarily normalized to the heights of the prominant peaks.

than 2 for neutral projectiles (data presented on linear scales). This we interpret with an enhanced fraction of projectiles that have performed 'skipping motion'. On the contrary, the intensities of energy loss structures in the spectra (not shown here) attributed to subsurface channelling are observed to be not affected by the charge state of the incoming projectile.

An increase in the 'skipping motion' yield for neutral projectiles has been observed also for scattering from a C(0001) surface (HOPG) by Stölzle (1995). In figure 25 we display yields obtained with 61 keV projectiles as a function of the energy for the transverse motion. It is interesting to note that the two data sets could be made to coincide by a shift

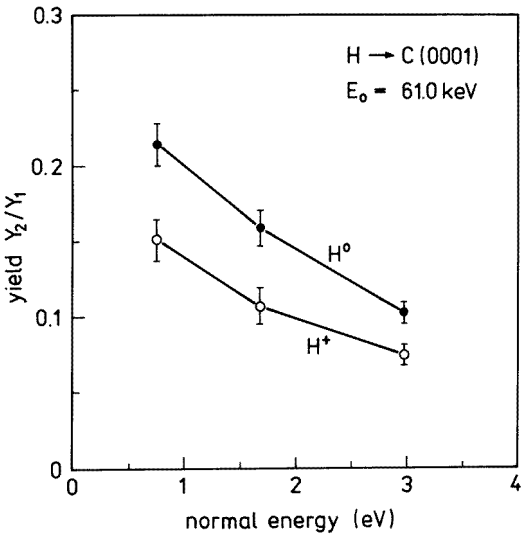

Figure 25. Ratios of yield Y_2/Y_1 for 61 keV projectiles scattered from C(0001) as a function of normal energy: ●, H atoms; ○, protons as projectiles; ——, lines drawn to guide the eyes. (From Stölzle (1995).)

in the transverse energy of about 1 eV. This can be considered as the gain in transverse energy of protons on the incident trajectory (the energy scale given in figure 25 refers to the 'macroscopic' incidence angle Φ_{in} without inclusion of image energies). From this feature these workers derive an effective distance for the onset of charge exchange: $z_s \approx 5$–6 au. This is a similar (somewhat too large) distance as derived from studies of angular distributions for Al(111).

In summarizing this section we can state that evidence for 'skipping motion' (similar to the everyday experience of the skipping of a flat stone across a water surface) has been obtained in a number of different experimental studies. Since the projectiles are bound to the surface via image charge effects, which depend on their charge states, detailed information is obtained on the dynamics of charge exchange processes close to solid surfaces. Furthermore, vibrational amplitudes and surface Debye temperatures might be deduced from the analysis of energy loss spectra as functions of target temperature (Ohtsuki 1991, Sakai *et al* 1992, Pfandzelter *et al* 1993).

5. Neutralization of multicharged ions

In the last few years the scattering of 'slow' multicharged ions from solid surfaces has been investigated by a number of different spectroscopic methods such as electron spectroscopy, electron emission statistics and yields, and x-ray spectroscopy. Progress in this field has been documented in a number of recent review papers (see, e.g., Das and Morgenstern (1993), Burgdörfer (1993), Aumayr and Winter (1994), Aumayr (1995), Zeijlmans van Emmichoven (1995), Burgdörfer *et al* (1996) and Winter (1996a).

The current status in the understanding of the very complex multielectron charge exchange problem of a multicharged ion in front of a solid can be summarized in terms of a classical 'over-barrier' model (Burgdörfer *et al* 1991). The main feature of this model is the resonant transfer of conduction electrons to highly excited electronic states of the

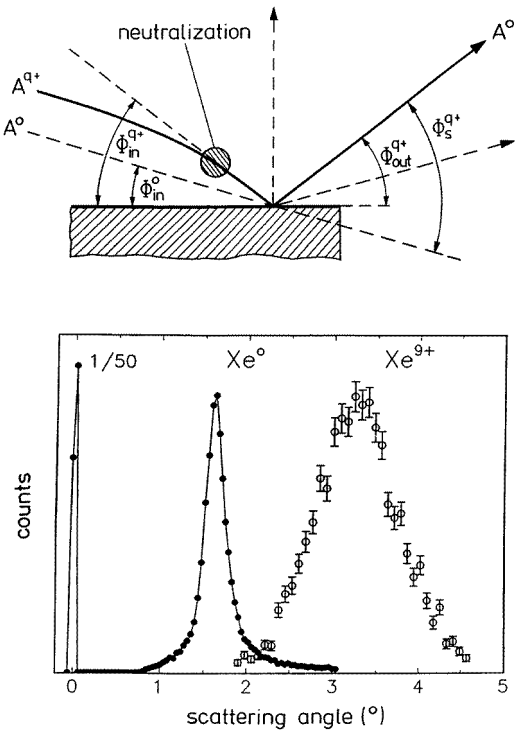

Figure 26. Sketch of image charge effects on the trajectory of a multicharged ion (upper part). Angular distributions of 25 keV Xe^0 (●) and Xe^{9+} (○) projectiles scattered from Al(111). The sharp and intense peak on the left side is due to projectiles that have passed above the target without scattering and serves as a reference for the scattering angle Φ_s.

atomic system. This results for a very short period of time in the formation of so-called 'hollow atoms', i.e. multiply excited atoms with most electrons in outer shells and a lack of population of inner shells. Because of the formation of these highly inverted atoms by resonant electron transfer processes, multicharged ions will be completely neutralized in front of the surface. However, the high Coulomb energy stored in the original projectile is still preserved in the first stage of interaction with the solid. This energy is liberated when the atoms reach the direct vicinity of the surface, where the loosely bound electrons are stripped off and the inner shells are filled in close encounters with target atoms and conduction electrons of high densities. This second stage of final neutralization is the subject of intense current research (see, e.g., Stolterfoht *et al* (1996)).

The effect of the image charge interaction on the trajectories of incident multicharged ions allows one to obtain important information on the neutralization sequence of the ions *in front* of the surface plane. This effect has been discussed already in section 4.3 for protons. Since image forces scale with the square of the projectile charge, the image interaction energies E_{im}^{q} and the resulting angular deflections are larger than for singly charged ions.

A sketch of the collision geometry and a typical result for 25 keV Xe^0 and Xe^{9+} projectiles scattered from Fe(110) under the same settings of the collimation and of the target are displayed in figure 26. For the neutral projectile we have specular reflection $\Phi_{in}^{0} = \Phi_{out}^{0} = \Phi_{s}^{0}/2$ so that $E_{0,z} = 25\ \text{keV}\sin^2(1.6^\circ/2) = 4.9$ eV, i.e. we have a

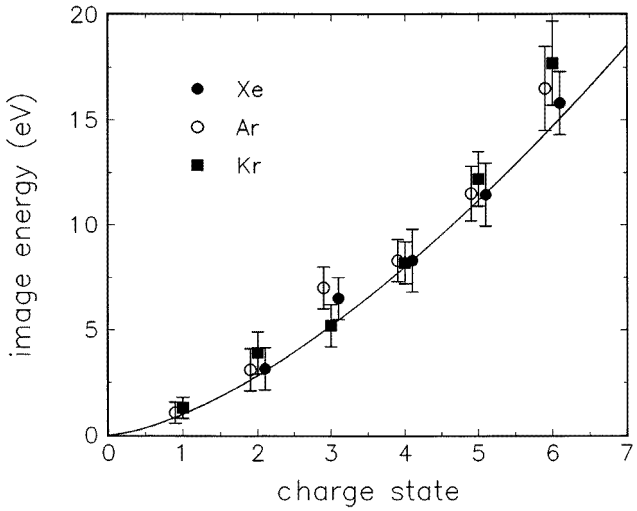

Figure 27. Energy gains as a function of the charge state of incident Xe (●), Ar (○) and Kr ions (■) deduced from angular distributions for 25 keV projectiles scattered at $\Phi_{in} \approx 1^\circ$.

'slow' particle with respect to the approach to the surface. Xe^{9+} projectiles are scattered at a clearly larger scattering angle $\Phi_s^q = 3.3^\circ$. An essential assumption of the method is complete neutralization of the projectile on the incident trajectory, so that no image charges affect the outgoing path and the neutralized projectiles can be considered to be scattered at effective incidence angles $\Phi_{in}^q > \Phi_{in}^0$. Then we find for the transverse energy $E_{q,z} = E_0 \sin^2(\Phi_s^q - \Phi_s^0/2) = 47.6$ eV, so that the ions have gained an energy $E_{im}^q = 42.7$ eV on the incident path (the uncertainty in E_{im}^q is some electronvolts).

This energy gain has two important aspects.

(1) It represents the lower limit of scattering energies of a projectile of charge q with the solid. The broadening of the angular distribution for the ions in figure 26 is primarily due to the enhanced transverse energies and the resulting corrugation of the scattering potential (Winter and Auth 1994).

(2) The image charge acceleration ceased owing to the (complete) neutralization of the projectile.

Thus E_{im}^q provides information on charge exchange processes and specifically on the distances from the surface, where these processes take place.

In figure 27 we show energy gains obtained for Kr^{q+}, Ar^{q+}, and Xe^{q+} ions in front of an Al(111) surface with $q \leqslant 6$. The data show the expected pronounced increase with increasing q and are within the experimental errors independent of the type of ion (Winter and Auth 1994). The solid curve in the figure represents energies obtained from a simple version of the 'over-barrier' model (Burgdörfer and Meyer 1993). This model treats the transfer of electrons between solid and ion in a classical manner. In figure 28(a) we have plotted the effective potential for an 'active' electron for an ion with core charge $Q = 6$ at a distance $R = 60$ au in front of a metal surface, characterized by a thick potential barrier that makes classically (and also quantum mechanically) electronic transitions between bound electronic states in metal and atom impossible. In figure 28(b) we show the same potential for $R = 15$ au and recognize a potential saddle which represents classically a pathway for

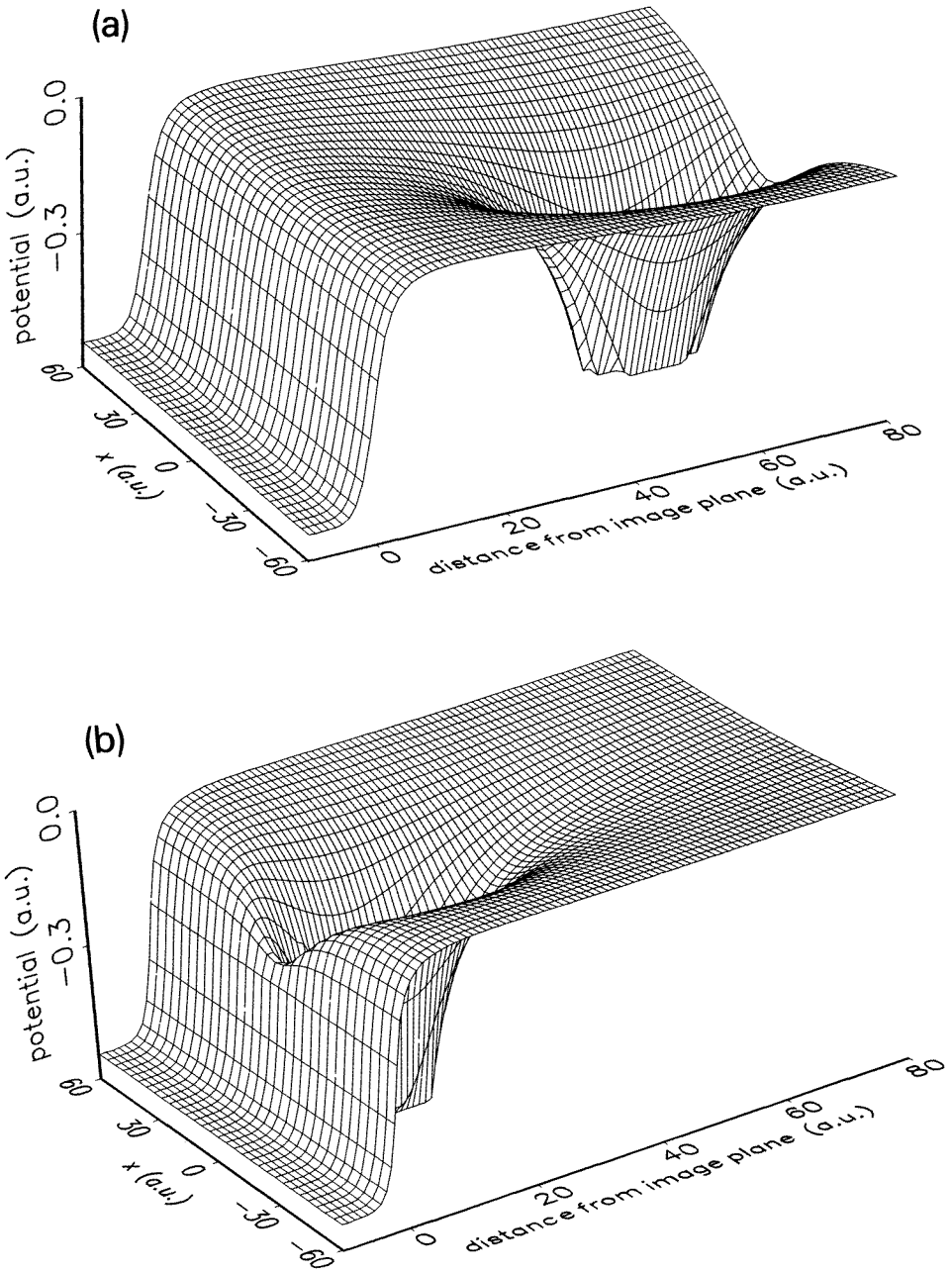

Figure 28. Effective potential for an 'active' electron for an ion core of charge $Q = 6$ in front of a metal surface: (a) $R = 60$ au, (b) $R = 15$ au.

electronic transitions.

In figure 29 a section of this potential on an axis along the surface normal containing the ion core (z-axis) and the contributions to the potential are sketched. The potential barrier

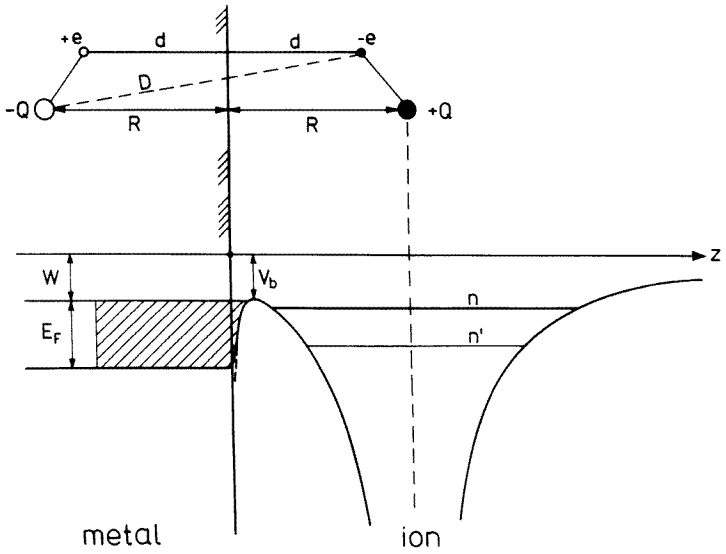

Figure 29. Sketch of the effective potential and its construction from the concept of static image charges in a direction along the surface normal through the ion core. In a classical picture, neutralization can take place when the potential barrier V_b is lowered to the Fermi level of the solid, i.e. $V_b > W$.

for distances R relevant for charge exchange of multicharged ions can be approximated by the concepts of image charges, i.e. in addition to the Coulomb potential of the ion core the 'active' electron interacts close to the surface with the image charge of the ion core and with its own image charge (see sketch in upper part of figure 29). For this description of the potential barrier the simple relation

$$V_b \approx \frac{\sqrt{2Q}}{R} \tag{10}$$

relates the height of the potential barrier to the distance R. In a classical picture, electrons can neutralize the ion, when the barrier is lowered to energies of occupied metal states, i.e. $V_b \geqslant W$. Then transitions of electrons to an ion approaching the surface with charge Q will proceed for distances

$$R_c \approx \frac{\sqrt{2Q}}{W} \tag{11}$$

which are relatively large. For a typical metal work function $W \approx 5$ eV, we get, for $Q = 10$, $R_c = 21.6$ au, where atomic states with principal quantum numbers $n \approx Q$ are populated. However, with the approach of ions towards the surface, level shifts and screening effects lower the binding energies, so that with a decreasing charge of the projectile the quantum number n of the occupied atomic states is also lowered with respect to the early stage of neutralization. A quantum-mechanical treatment of electronic transition rates by Borisov *et al* (1996a, b) for the $n = 9$ manifold of O^{7+} ions demonstrates a further complexity of the problem; levels of the manifold are strongly mixed by the electric dipole of the image charges (see figure 29) and Stark hybrids are formed with electronic densities displaced to the region between the surface and the ion core and with quite different transition rates and energy shifts of atomic levels.

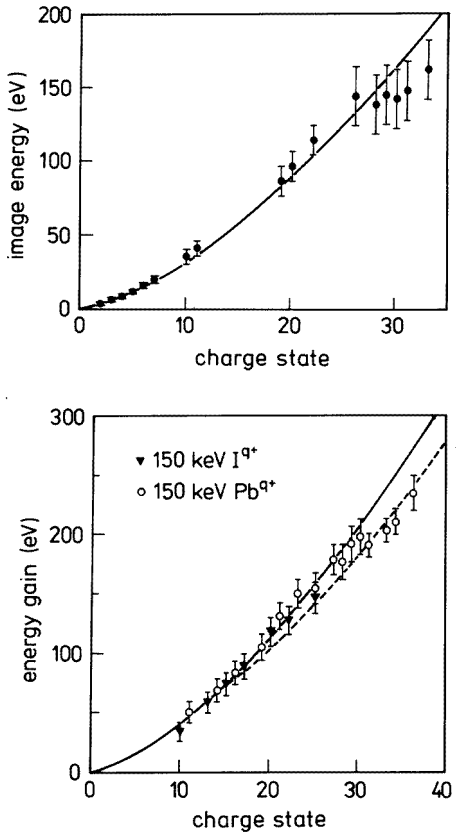

Figure 30. Energy gains of multicharged ions in front of metal surfaces: upper figure: Xe^{q+} ions in front of Al(111) (Winter *et al* 1993); lower figure, I^{q+} and Pb^{q+} ions in front of Au(110) (Meyer *et al* 1995).

A simple approximation for the description of the complex neutralization dynamics is the 'staircase model' of subsequent electron capture. The charge state of the projectile is reduced by one at distances $R_c(Q)$ given by equation (11) to the effective charge $Q-1$, which is preserved to a distance $R_c(Q-1)$. From the classical limit for the image interaction energy $-q^2/4R$, we deduce for the energy gain of an ion with initial charge Q that

$$E_{im}^{Q} = \sum_{q=1}^{Q} \frac{2q-1}{4R_c(q)} \approx \frac{W}{3\sqrt{2}} Q^{3/2}. \tag{12}$$

The simple model reproduces the data, shown in figure 27 by a solid curve on a quantitative level. Also the (linear) scaling with the work function W observed for different metal targets and alkali adsorption as well as the insensitivity on atomic species are in agreement with the model.

In experiments with higher charges, the $Q^{3/2}$ dependence of E_{im}^{Q} is well reproduced up to charge states $Q \approx 30$ as can be seen in figure 30 which shows data for Xe^{q+} on Al(111) (Winter *et al* 1993) and for I^{q+} and Pb^{q+} on Au(110) (Meyer *et al* 1995). However, for $Q > 30$ a clear deviation from $Q^{3/2}$ (solid curve) is evident in both data sets obtained with different sorts of projectile and target. This deviation is remarkable also in the sense that

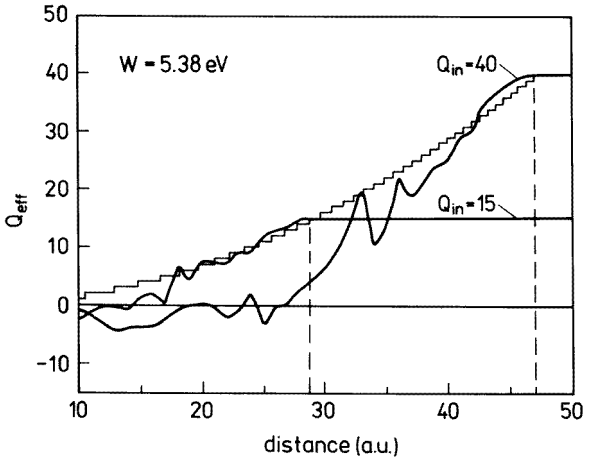

Figure 31. Effective charge Q_{eff} of a multicharged ion as a function of the distance from a Au surface ($W = 5.38$ eV) for $Q_{in} = 15$ and $Q_{in} = 40$: stepped curve, 'staircase model'; solid curves, 'over-barrier' model calculations by Lemmell *et al* (1996).

energy gains obtained with larger uncertainties from saturation effects of electron emission yields follow $Q^{3/2}$ up to $Q = 79$ (Kurz *et al* 1994).

In a recent paper by Lemell *et al* (1996) a convincing explanation for the observed effect is presented. In detailed classical simulations based on the 'over-barrier' approach, these workers found that, for very high charge states, pronounced deviations from the staircase model arise because hollow atoms can accommodate an excess number of electrons owing to incomplete screening within the atom. The effect leads for high initial charges to a faster reduction in the effective projectile charge. In figure 31 a result of the simulations for $Q_{in} = 15$ and 40 is shown. Whereas for $Q_{in} = 15$ the neutralization sequence proceeds via effective charges that follow rather closely the staircase model, for $Q_{in} = 40$ the ions clearly have smaller charges at smaller distances. This reduction in effective charge also reduces the energy gain as observed in the experiments. The broken curve in figure 30 represents energy gains derived from the simulations for a Au surface and is in good agreement with the data.

In conclusion, we can state that the study of image charge effects on the trajectories of multicharged ions in front of solid surfaces provides important information on the neutralization dynamics that allows one to locate the relevant electron capture events. Recently, evidence for the formation of 'hollow atoms' has also been obtained for grazing scattering from insulators (Auth *et al* 1995, Auth and Winter 1996). For the neutralization of multicharged ions in front of insulator surfaces the potential barrier has to be lowered to energies of valence band electrons (typically 10 eV for alkali halides), so that $R_c(Q)$ is smaller than for metal targets. Since on the other hand the dielectric response is reduced, experiments on the scattering from surfaces of ionic crystals give energy gains as comparable with those observed for metals.

6. Scattering of helium atoms and ions from an Al(111) surface

We shall close this brief review with a discussion of two recent experiments on the scattering of He atoms in ground and metastable states as well as He^+ ions from an Al(111) surface.

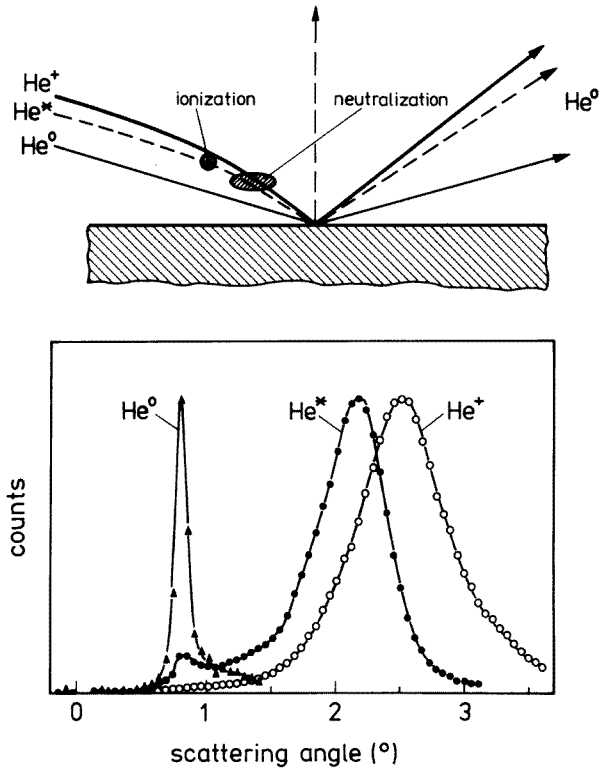

Figure 32. Sketch of the trajectories of He projectiles in front of a metal surface, where the shaded areas indicate intervals of ionization of incident metastable atoms and of Auger neutralization of the He^+ ion, respectively. The lower part shows experimental distributions for incident 4 keV He atoms (▲), metastable He atoms (●) and He^+ ions (○). The data are arbitrarily normalized.

In figure 32 we have sketched the trajectories of He^0, He^*, and He^+ projectiles and present in the lower part of the figure experimental angular distributions for projectile energies $E_p = 4$ keV (Hecht 1996). For these energies no electron loss mechanism is present (Winter 1993b), so that He^0 projectiles (produced in a gas target operated with air) will stay neutral over their complete trajectories and are scattered with a well defined angular distribution in specular direction.

For He^+ ions, image charge effects shift and broaden the angular distributions significantly. In the same manner as discussed in the previous sections, one can analyse the data with respect to neutralization processes, i.e. rates for Auger neutralization of the incoming He^+ ion (Hagstrum 1954). Evaluation of data allows one to deduce reliable rates (Winter 1993a, Hecht 1996) for comparison with theoretical calculations, revealing a pronounced dependence of Auger rates on the modelling of the potential barrier (Fondén and Zwartkruis 1992, Lorente *et al* 1994).

When the projectile beam is neutralized in an alkali-vapour cell, quasi-resonant charge exchange leads for kiloelectronvolt ions to predominant populations of the metastable $2\,^1S$ and $2\,^3S$ terms. These terms have binding energies lower than the work function of Al(111) and are thus ionized by resonant electronic transitions of the 2s electron to an unoccupied conduction state. From this instant, the He^* atoms are converted to He^+ ions and attracted

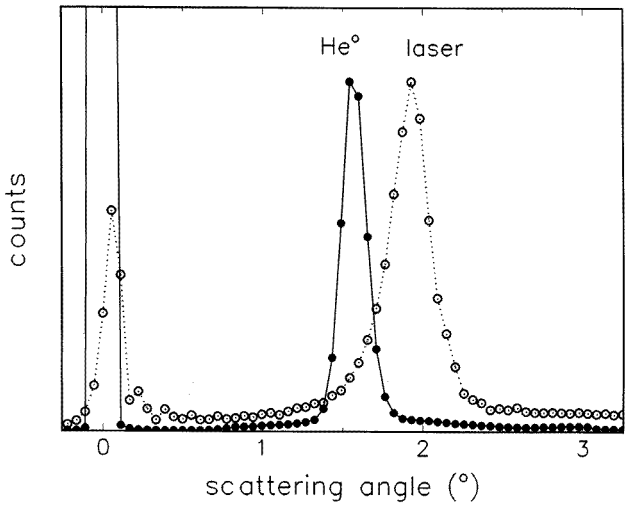

Figure 33. Angular distributions for 4 keV He atoms (●) and for He–Ne laser light (○) after scattering and specular reflection from an Al(111) surface.

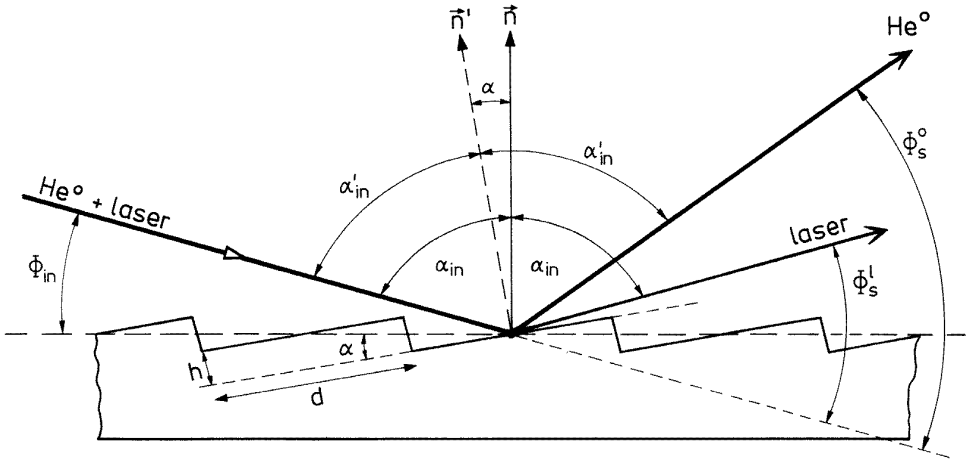

Figure 34. Sketch of the geometry for the scattering of atoms and laser light from a regularly stepped surface.

via the image force until the He^+ ions are neutralized via an Auger-process. This leads to slightly smaller total energy gains than for incoming ions as shown in the reduced angular deflection in figure 32. From these data, transition rates can be derived for the resonant ionization of the 2s terms.

An interesting aspect of the data is based on the small peak in the distribution for He^* projectiles at the scattering angle for He^0 atoms. This feature is simply attributed to the fraction of atoms in the $1s^2\ ^1S$ ground-state term within the metastable beam. In this respect, the angular distributions can be made use of as a 'detector' for the ratio of populations in stable and metastable terms. The analysis of the data shown in the figure yields a fraction of about 3% ground-state term atoms in the neutral beam (Hecht 1996).

An important additional effect on trajectories is observed in these experiments for He^0 projectiles, when the angular distributions for scattered atoms as well as for scattered light of a He–Ne laser beam collimated by the same settings of the slits are recorded. The well defined distributions show a small but systematic angular shift (figure 33) which is independent of the angle of scattering; however, it reverses for a 180° azimuthal rotation of the target (Hecht *et al* 1996).

We interpret this finding by the feature that a stepped target surfaces acts as an 'echelette-grating' (Comsa *et al* 1979), where the laser light with a wavelength ($\lambda = 623$ nm) larger than the terrace width d is scattered from the 'macroscopic' surface plane (figure 34). The fast atoms, however, are scattered with respect to the planes of single terraces. Thus, from the angular shift between laser and fast atomic beam, the angular misfit between crystallographic planes and the surface can be deduced, and terrace widths can be estimated. From the observed angular shift $\Delta\Phi = 0.4°$ we deduce an averaged terrace width $d \approx h/\tan(\Delta\Phi/2) \approx 70$ nm for a monatomic step height $h = 0.234$ nm for Al(111) (Hecht *et al* 1996). This estimate on d is consistent with a SPALEED analysis performed on a comparable Al(111)-sample.

Acknowledgments

The assistance of Mrs M Janetzki and A Bensch in processing the manuscript is gratefully acknowledged. I thank Professor I Tsong and Dr R Pfandzelter for a critical reading of the manuscript. This work is supported by the Deutsche Forschungsgmeinschaft in the Sonderforschungsbereich 216 (Bielefeld/Münster) and under contract Wi 1336/1-1.

References

Arista N R 1994 *Phys. Rev.* A **49** 1995
Annett J F and Echenique P M 1986 *Phys. Rev.* B **34** 6853
Aumayr F 1995 *The Physics of Electronic and Atomic Collisions, Proc. 19th Int. Conf. on the Physics of Electronic and Atomic Collisions (AIP Conf. Proc. 360) (Woodbury, 1995)* ed L J Dubé *et al* (New York: American Institute of Physics) p 631
Aumayr F and Winter H P 1994 *Comments At. Mol. Phys.* **29** 275
Auth C, Hecht T, Igel T and Winter H 1995 *Phys. Rev. Lett.* **74** 5244
Auth C and Winter H 1996 *Phys. Lett.* **217A** 119
Borisov A G, Winter H, Dierkes G and Zimny R 1996a *Europhys. Lett.* **33** 229
Borisov A G, Zimny R, Teillet-Billy D and Gauyacq J P 1996b *Phys. Rev.* A **53** 2457
Burgdörfer J 1993 *Progress in Atomic and Molecular Physics* ed C D Lin (Singapore: World Scientific) p 517
Burgdörfer J, Lerner P and Meyer F 1991 *Phys. Rev.* A **44** 5674
Burgdörfer J and Meyer F 1993 *Phys. Rev.* A **47** R20
Burgdörfer J, Reinhold C, Hägg L and Meyer F 1996 *Aust. J. Phys.* **49** 527
Comsa G, Mechtesheimer G, Poelsema B and Tomoda S 1979 *Surf. Sci.* **89** 123
Cooper B H and Behringer E R 1994 *Low Energy Ion–Surface Interactions* ed J W Rabalais (Chichester: Wiley) p 263
Das J and Morgenstern R 1993 *Comments At. Mol. Phys.* **29** 205
Echenique P M and Howie A 1984 *Ultramicroscopy* **16** 269
Eisen F H and Robinson M T 1971 *Phys. Rev.* B **4** 1457
Eguiluz A G and Hanke W 1989 *Phys. Rev.* B **39** 10 433
Fondén T and Zwartkruis A 1992 *Surf. Sci.* **269–70** 601
Garcia de Abajo F J and Echenique P M 1992 *Phys. Rev.* B **46** 2663
Geerlings, J J C, Los J, Gauqacq J P and Temme N M 1986 *Surf. Sci.* **172** 257
Gemmell D S 1974 *Rev. Mod. Phys.* **46** 129
Hagstrum H D 1954 *Phys. Rev.* **96** 336
Hecht T 1996 *Diploma Thesis* Humboldt-Universität zu Berlin
Hecht T, Auth C and Winter H 1996 *Nucl. Instrum. Methods* B submitted

Hentschke, R, Snowdon K J, Hertel P and Heiland W 1986 *Surf. Sci.* **173** 565
Jackson J D 1975 *Classical Electrodynamics* 2nd edn (New York: Wiley) p 54
Kaminski M 1965 *Atomic and Ionic Impact Phenomena on Metal Surfaces* (Berlin: Springer)
Kato M, Iitaka T and Ohtsuki Y H 1988 *Nucl. Instrum. Methods.* B **33** 432
Kato M and Snowdon K J 1994 *Nucl. Instrum. Methods.* B **90** 80
Kimura K, Hasegawa M and Mannami M 1987 *Phys. Rev.* B **36** 7
Kurz H, Aumayr F, Winter H P, Schneider D, Briere M A and McDonald J W 1994 *Phys. Rev.* A **49** 4639
Lemell C, Winter H P, Aumayr F, Burgdörfer J and Meyer F 1996 *Phys. Rev.* A **53** 880
Lorente N 1995 *Thesis* University of Madrid
Lorente N, Monreal R and Alducin M 1994 *Phys. Rev.* A **49** 4716
Los J and Geerlings J J C 1990 *Phys. Rep.* **190** 133
Lundqvist V I 1986 *Chem. Scr.* **26** 423
Lutz H O, Datz S, Moak C O and Noggle T S 1966 *Phys. Rev. Lett.* **17** 285
Meyer F, Folkerts L, Folkerts H O and Schippers S 1995 *Nucl. Instrum. Methods* B **98** 441
Miskovic Z, Vukanic J and Madey T E 1984 *Surf. Sci.* **141** 285
Muscat J P and Newns D M 1979 *Phys. Rev.* B **19** 1270
Narumi K, Fujii Y and Kimura K 1994a *Nucl. Instrum. Methods* B **90** 266
Narumi K, Fujii Y, Kimura K and Mannami M 1994b *Surf. Sci.* **303** 187
Newns D M 1989 *Comm. Condens. Matter Phys.* **14** 295
Nienhaus H 1988 *Diploma Thesis* Münster
Nordlander P 1992 private communication
Nordlander P and Tully J C 1988 *Phys. Rev. Lett.* **61** 990
——1989 *Surf. Sci.* **211–12** 207
Ohtsuki Y H 1983 *Charged Beam Interaction with Solids* (London: Taylor & Francis) p 233
——1991 private communication
Ohtsuki Y H, Koyama K and Yamamura Y 1979 *Phys. Rev.* B **20** 5044
Overbosch E G, Rasser B, Tenner A D and Los J 1980 *Surf. Sci.* **92** 310
Pfandzelter R, Stölzle F, Sakai H and Ohtsuki Y H 1993 *Nucl. Instrum. Methods.* B **83** 469
Raskin D and Kusch P 1968 *Phys. Rev.* **179** 712
Sakai H, Iitaka T and Ohtsuki Y H 1992 *Phys. Lett.* **161A** 467
Sakai H, Yamashita R and Ohtsuki Y H 1995 *Nucl. Instrum. Methods* B **96** 494
Snowdon, K J, O'Connor D J and MacDonald R J 1988 *Phys. Rev. Lett.* **61** 1760
——1989 *Surf. Sci.* **221** 465
Sommer M 1991 *Diploma Thesis* Münster
Stölzle F 1995 *Thesis* Universität München
Stölzle F and Pfandzelter R 1990 *Phys. Lett.* **150A** 315
——1991 *Surf. Sci.* **251** 383
——1992 *Europhys. Lett.* **20** 369
Stolterfoht N, Niemann D, Grether M, Spieler A and Arnau A 1996 *Scanning Microsc. Int.* at press
Wilke, M 1994 *Diploma Thesis* Universität Münster
Winter H 1991 *Comments At. Mol. Phys.* **26** 287
——1992a *Phys. Rev.* A **46** R13
——1992b *Europhys. Lett.* **18** 207
——1993a *J. Phys.: Condens. Matter* **5** A295
——1993b *Nucl. Instrum. Methods* B **78** 38
——1996a *Rev. Sci. Instrum.* **67** 1420
——1996b to be published
Winter H and Auth C 1994 *Nucl. Instrum. Methods* B **90** 216
Winter H, Auth C, Schuch R and Beebe E 1993 *Phys. Rev. Lett.* **71** 1939
Winter H and Borisov A G 1996 *Nucl. Instrum. Methods* B **115** 211
Winter H and Leuker J 1992 *Nucl. Instrum. Methods* B **72** 1
Winter H, Leuker J, Sommer M and Ortjohann H W 1992 *Proc. Werner Brandt Workshop on Charged Particle Penetration Phenomena (Oak Ridge, TN, 1992) ORNL Report* p 38
Winter H and Sommer M 1992 *Phys. Lett.* **168A** 409
Zeijlmans von Emmichoven P 1995 *Physics with Multiply Charged Ions* ed D Liesen (New York: Plenum) p 263
Ziegler J F, Biersack J P and Littmark U 1985 *The Stopping and Range of Ions in Solids* vol 1 (Oxford: Pergamon)
Zimny R, Miskovic Z L, Nedeljkovic N N and Nedeljkovic L C 1991 *Surf. Sci.* **255** 135
Zimny R, Nienhaus H and Winter H 1989 *Radiat. Effects and Defects Solids* **109** 9